A modeling study of the interaction between the Atlantic Warm Pool, the tropical Atlantic easterlies, and the Lesser Antilles

Steven C. Chan,[1] Vasubandhu Misra,[1,2] and H. Smith[3]

Received 27 October 2010; revised 31 January 2011; accepted 9 February 2011; published 20 April 2011.

[1] The European Centre for Medium-Range Forecasts Reanalysis-40 and National Centers for Environmental Prediction (NCEP)/Department of Energy reanalyses are downscaled over the eastern Caribbean and Lesser Antilles using the NCEP-Scripps Regional Spectral Model for Augusts when the Atlantic Warm Pool (AWP) area is the most anomalous. The simulations show a two-way influence between the Lesser Antilles and the AWP: the islands modulate the regional atmospheric circulation, and AWP variations modulate the interannual variabilities of the islands. The Lesser Antilles introduce diurnal variations and drag to the easterlies. The presence of the islands modulates the prevalent easterlies as a result of the daytime heating of the islands and the consequent boundary layer expansion. The modulations are sensitive to the islands' size and topography. Small and flat islands act as thermal plumes, but the modulations of large and hilly islands are during the daytime as their boundary layer expands. The manifestation of the atmospheric response to the sea surface temperature (SST) anomalies over the islands is sensitive to the island orography. For most islands, the atmospheric response to the SST anomalies is reflected only during the daytime. For all one-grid-point islands and Antigua, nighttime and dawn minimum temperatures are modulated to the same degree as the daytime maximum. For island rainfall, downscaling reduces the gross overestimations of rainfall in the reanalyses. However, our downscaling results suggest that there is room for improvement in simulating the marine surface diurnal cycle.

Citation: Chan, S. C., V. Misra, and H. Smith (2011), A modeling study of the interaction between the Atlantic Warm Pool, the tropical Atlantic easterlies, and the Lesser Antilles, *J. Geophys. Res.*, *116*, D00Q02, doi:10.1029/2010JD015260.

1. Introduction

[2] The Atlantic Warm Pool (AWP) is a pool of tropical warm water that forms during the boreal summer/fall season over the Gulf of Mexico, the Caribbean Sea, and the tropical western Atlantic [*Wang and Enfield*, 2001]. The AWP is part of the greater Western Hemisphere Warm Pool (WHWP), which includes both the tropical eastern Pacific and the Atlantic. The extent of the WHWP/AWP is defined as the area enclosed by the 28.5°C SST isotherm. The WHWP area tends to be largest during the late boreal summer season between August and September.

[3] A low-level easterly jet called the Caribbean low-level jet (CLLJ) [*Stensrud*, 1996; *Mo et al.*, 2005; *Muñoz et al.*, 2008] (hereinafter M08) overlies the AWP in the Caribbean. Unlike the AWP, which has only one seasonal maximum, the CLLJ has two: one in the boreal winter and another in the boreal summer. Here, we concern ourselves only with the boreal summer, when the AWP area is the largest. The CLLJ transports tropical Atlantic moisture westward toward the Gulf of Mexico, where it meets with the Great Plains low-level jet (GPLLJ). The latter transports moisture into the continental United States and Canada [*Rasmusson*, 1967; *Bosilovich and Schubert*, 2002]. The rainfall peaks in the tropical Caribbean and continental Central America during the boreal summer (with a drier midsummer period); however, rainfall over the Caribbean Sea is generally lower than rainfall over tropical continental Central America and the tropical East Pacific [*Magaña et al.*, 1999].

[4] The interannual variability of the boreal summer CLLJ easterlies is connected with the AWP through the movement of the North Atlantic sea level subtropical high [*Wang*, 2007]. The CLLJ is located on the southern flank of the Bermuda High. Large (small) AWP is associated with weaker (stronger) CLLJ easterlies and lower (higher) sea level pressure over the Caribbean. *Cook and Vizy* [2010] (hereinafter CV10) show strong LLJ (small AWP) is related to reduced rainfall over the boreal summer Caribbean.

[5] Many studies have investigated the relationship between the prevailing AWP variability and broader regional climate [*Wang*, 2007; *Wang and Lee*, 2007; *Cook and Vizy*, 2010]. *Wang and Lee* [2007] posit that an increase in Atlantic hurricane activity occurs when AWP is larger.

[1]Center for Ocean-Atmospheric Prediction Studies, Florida State University, Tallahassee, Florida, USA.
[2]Department of Earth, Ocean, and Atmospheric Sciences, Florida State University, Tallahassee, Florida, USA.
[3]Water Resources Research Institute, University of the Virgin Islands, St. Thomas, Virgin Islands, USA.

0148-0227/11/2010JD015260

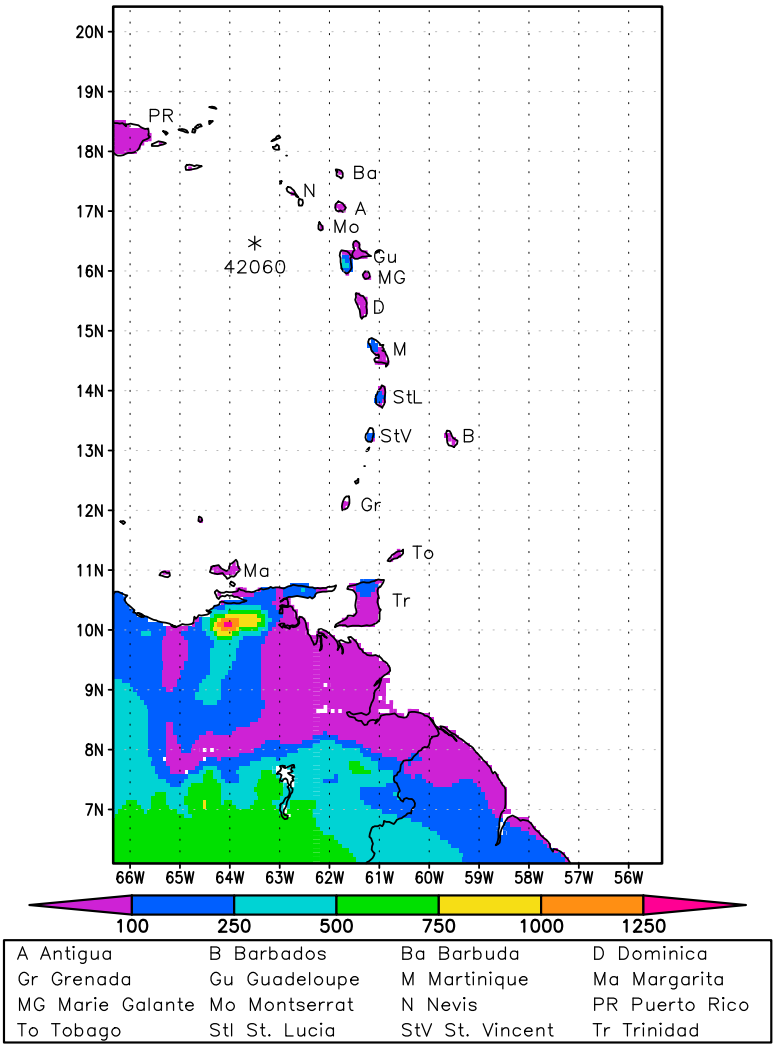

Figure 1. The domain used in the regional climate simulation. Major islands and surface topography are shown. Water pixels are white. NDBC buoy 42060s coordinate (see section 7) is marked with an asterisk.

CV10 show a link between CLLJ variability and precipitation over the United States in the boreal winter. The relationship, however, does not exist during the boreal summer when AWP is prominent because of the weaker changes in the zonal sea level pressure gradients associated with the north Atlantic subtropical anticyclone.

[6] Because of the small size of some of the Caribbean islands (especially in the Lesser Antilles), most global climate models simply cannot resolve the islands. Here we seek to understand the following: (1) the islands' impact on the regional climate and (2) the AWP/CLLJ variability modulation of the islands' climate variability. This is accomplished with a high-resolution regional dynamical model in which the relatively small islands are explicitly resolved. *Amador* [2008] showed that downscaling reanalyses improve the representation of the lower troposphere winds. Here we chose the National Centers for Environmental Prediction (NCEP)-Scripps Institution of Oceanography (SIO) Regional Spectral Model (RSM) [*Juang and Kanamitsu*, 1994; *Kanamaru and Kanamitsu*, 2007].

[7] The island can interact with the surrounding water only through the atmosphere. The interaction of the prevailing low-level easterlies with the islands may occur at the mesoscale level through the island's orography and diurnal variations. The heating-forced convective mixing [*Holton*, 2004], sea/land breezes caused by temperature contrasts, and the drag on the atmospheric flow from the island's topography and land cover [*Smith et al.*, 1997; *Carbone et al.*, 2000] are examples of possible interactions.

[8] Focusing only on topography interaction, *Grubišić et al.* [1995] and *Smith et al.* [1997] showed that the island shapes impact the turbulent wake generated. In our RSM simulations, the Lesser Antilles have less topography than in reality (see Figure 1 and compare with Figure 2 of *Smith et al.* [1997]); however, the RSM is a major improvement from having no islands at all in coarse-grid models.

[9] Section 2 of this paper discusses the major components of the RSM and the data used in the study. Section 3 gives a broad overview of the interannual variability of the AWP. Section 4 describes the simulated island impacts on the sur-

Table 1. The Lesser Antilles Resolved by RSM, Their Approximate Coordinates, and the Number of Grid Points the Islands Occupy[a]

Island Name	Latitude and Longitude	Number of Grid Points	Number of Grid Points Along *y*
Barbados	59.6°W 13.3°N	5	3
Tobago	60.7°W 11.3°N	4	3
Grenada	61.8°W 12.1°N	3	2
St. Vincent	61.3°W 13.3°N	4	2
St. Lucia	*61.0°W 13.9°N*	*11*	*5*
Martinique	*61.1°W 14.7°N*	*16*	*6*
Dominica	*61.5°W 15.4°N*	*12*	*6*
Marie Galante	61.3°W 15.9°N	3	2
Guadeloupe	*61.5°W 16.3°N*	*27*	*8*
Montserrat	**62.2°W 16.8°N**	**1**	**1**
Antigua	61.8°W 17.1°N	5	2
Barbuda	**61.8°W 17.6°N**	**1**	**1**
Nevis	**62.8°W 17.3°N**	**1**	**1**
Trinidad	*61.3°W 10.5°N*	*78*	*11*

[a]Islands that occupy only one grid point and 10+ grid points are in boldface and italics, respectively. Antigua is noted for its unique interannual variability (see section 5).

rounding marine environment. In section 5, we describe how interannual AWP variability forces changes to the Lesser Antilles. Section 6 intercompares the simulated rainfall with corresponding observations and reanalyses; section 7 presents in situ observations in the Lesser Antilles. Finally, section 8 contains the conclusions.

2. Models and Data

2.1. AWP Sea Surface Temperatures

[10] National Oceanic and Atmospheric Administration (NOAA) Extended Reconstruction Sea Surface Temperature analysis version 3 (ERSST) [*Smith et al.*, 2008] is used to compute the AWP area. The AWP area is computed by summing the area covered by pixels with SST higher than 28.5°C in the Atlantic, the Caribbean, and the Gulf of Mexico between 0°N and 40°N. For RSM forcing, we have used the daily averaged (diurnally invariant) European Centre for Medium-Range Forecasts (ECMWF) SSTs [*Fiorino*, 2004].

2.2. Atmospheric Reanalysis

[11] The ECMWF Reanalysis 40 (ERA-40) [*Uppala et al.*, 2005] and the National Centers for Environmental Prediction (NCEP)/Department of Energy (DOE) [*Kanamitsu et al.*, 2002] reanalysis (hereinafter NCEPR2) are used to force the RSM. ERA-40 is available from September 1957 to August 2002. The assimilating model for ERA-40 is the ECMWF operational model that was in operation between June 2001 and January 2002. The ERA-40 assimilating model uses Tiedtke convection parameterization [*Tiedtke*, 1989, 1993] and updated land surface and PBL schemes that lead to improvements in high-latitude surface temperatures. The input data for ERA-40 include upper air observations from fixed stations and aircraft, surface station observations, and various remote sensing data. NCEPR2 is available for all months since January 1979. NCEPR2 is an update to the NCEP/National Center for Atmospheric Research (NCAR) reanalysis [*Kalnay et al.*, 1996], with improvements to the land surface and hydroclimate of the NCEP/NCAR reanalysis. The assimilating model is the NCEP Global Forecast System (GFS). The version of GFS that is used for NCEPR2 uses the *Hong and Pan* [1996] PBL scheme and the simplified Arakawa-Schubert cumulus scheme [*Hong and Pan*, 1998]. Upper air observations assimilated into the NCEPR2 are similar to those of ERA-40 (J. Wollen, NCEP, personal communication, 2010).

[12] Detailed reanalyses intercomparisons are beyond the scope of this paper. Both reanalyses use mass flux convection and (corrected) K-theory boundary layer schemes. For the tropics, *Nigam et al.* [2000] and *Chan and Nigam* [2009] have intercompared the time mean and interannual variations of diabatic heating (an integral measure of the general circulation and convection in the tropics, sensitive to the assimilating model cumulus and boundary layer parameterization) between ECMWF and NCEP reanalyses. ECMWF reanalyses are found to have more intense time mean and interannual varying tropical circulations.

2.3. NCEP-SIO RSM

[13] The NCEP-SIO RSM [*Juang and Kanamitsu*, 1994] is a regional dynamic atmosphere-land coupled climate model. RSM has undergone significant changes since its inception in the 1990s, including the introduction of the scale selective bias correction (SSBC) [*Kanamaru and Kanamitsu*, 2007] to the model's atmospheric component. The standard SSBC nudges vorticity in spectral space toward large-scale forcing data only in wavelengths larger than 1000 km, and forces domain mean moisture and temperature perturbations to zero. In our simulations, the horizontal nudging scale is reduced to 400 km owing to the small size of the regional domain and high horizontal resolution. Apart from SSBC, reanalyses are nested into the RSM at 6 h intervals in a six-point sponge zone around the lateral boundaries of the regional domain.

[14] RSM uses the updated Kain-Fritsch cumulus convection scheme [*Kain and Fritsch*, 1990; *Kain*, 2004] (hereinafter KF-C) and PBL scheme by *Hong and Pan* [1996] (same as in NCEPR2; hereinafter HP-PBL). The RSM land surface component is the recently developed NOAH (NCEP-Ohio State-U.S. Air Force-NWS Hydrology Laboratory) LSM [*Ek et al.*, 2003]. The KF-C scheme is a mass flux scheme with convective downdrafts physics. Convection is triggered when unstable updraft source layers are found with the search beginning at the lowest model vertical layer. Closure is assumed when 90% of the convective available potential energy (CAPE) is removed. The HP-PBL scheme takes into account PBL mixing due to both local gradient and "large-scale" eddies (K-theory "diffusive" gradient-based turbulent flux plus a "large eddy" correction). The PBL height (hereinafter H_{PBL}) is determined recursively by incrementally changing H_{PBL} until the Richardson number (Ri) matches with a specified critical value ($Ri_{cr} = 0.5$).

[15] RSM simulations are carried out at 8 km horizontal resolution with a 20 s time step and 28 vertical sigma-pressure levels. The Lesser Antilles isles resolved at 8 km are shown in Table 1. Upper atmosphere and single-layer (including 2 m temperature) outputs are available at 3 h and 1 h intervals, respectively. The simulation domain is shown in Figure 1. The domain covers the eastern Caribbean, the Lesser Antilles, and parts of South America and the Greater Antilles. The islands are relatively flat compared to

Table 2. Years Selected for RSM Downscaling Simulations[a]

	Years
Simulated Large AWP	1987, 1995, 1998, and 1999
Simulated Small AWP	1984, 1986, 1992, and 1994

[a]The selection criterion is that the AWP area for the year has to be ±1 standard deviation from the 1979–2001 mean.

Table 3. The Average, Median (and the Year of Occurrence), and Standard Deviation of AWP Area for JJA, August, and ASO

	Mean (km^2)	Median (km^2), (Year)	SD (km^2)
JJA	4.19×10^6	3.75×10^6, 1979	1.84×10^6
August	6.98×10^6	6.57×10^6, 1983	2.20×10^6
ASO	6.53×10^6	6.28×10^6, 1996	2.45×10^6

continental South America; only Guadeloupe has "surface topography" higher than 250 m. The core of the CLLJ is located at the west end of the domain, and our domain extends westward to the eastern LLJ entrance (see Figure 4).

[16] The simulations are carried out for August for the four small and four large AWP years listed in Table 2. All simulations begin on 0000 UT 29 July of the specified year. Initial soil conditions are given by NCEPR2 surface analyses.

2.4. Precipitation Analyses and Other Data Used

[17] We have employed two precipitation analyses. For "historical" comparisons (between large and small AWPs), the Climate Prediction Center merged analysis of precipitation (CMAP) is used [*Xie and Arkin*, 1997]. This CMAP version does not assimilate NCEP/NCAR reanalysis. When interannual variability is irrelevant, the 3-hourly and monthly (3B-42/43) 0.25° resolution merged Tropical Rainfall Measuring Mission (TRMM) analyses [*Huffman et al.*, 2007] are used.

[18] NOAA buoy and upper atmospheric sounding observations are used as well [*Hamilton*, 1986; *Durre et al.*, 2006]. The observations are local "point" measurements, and differ fundamentally with area-averaged gridded data sets (such as precipitation and model analyses). However, insights can be gained from the "point" in situ observations as they represent the best estimate to the ground truth.

3. Interannual AWP Variations and Their Atmospheric Signatures

[19] The interannual variations of the June-July-August (JJA), August, and August-September-October (ASO) AWP areas between 1979 and 2001 are summarized in Figure 2 and in Tables 2 and 3. We have selected the Augusts when AWP areas are ±1 standard deviation from the 1979–2001 mean for downscaling.

[20] August AWP areas are highly correlated (0.8+; not shown) with both JJA and ASO seasonal AWP areas. Therefore, August is a representative month of AWP forcing for downscaling. The prescribed ERA SST differences between the large and small AWP Augusts in our domain are shown in Figure 3a. SSTs are about 1°C lower in the selected

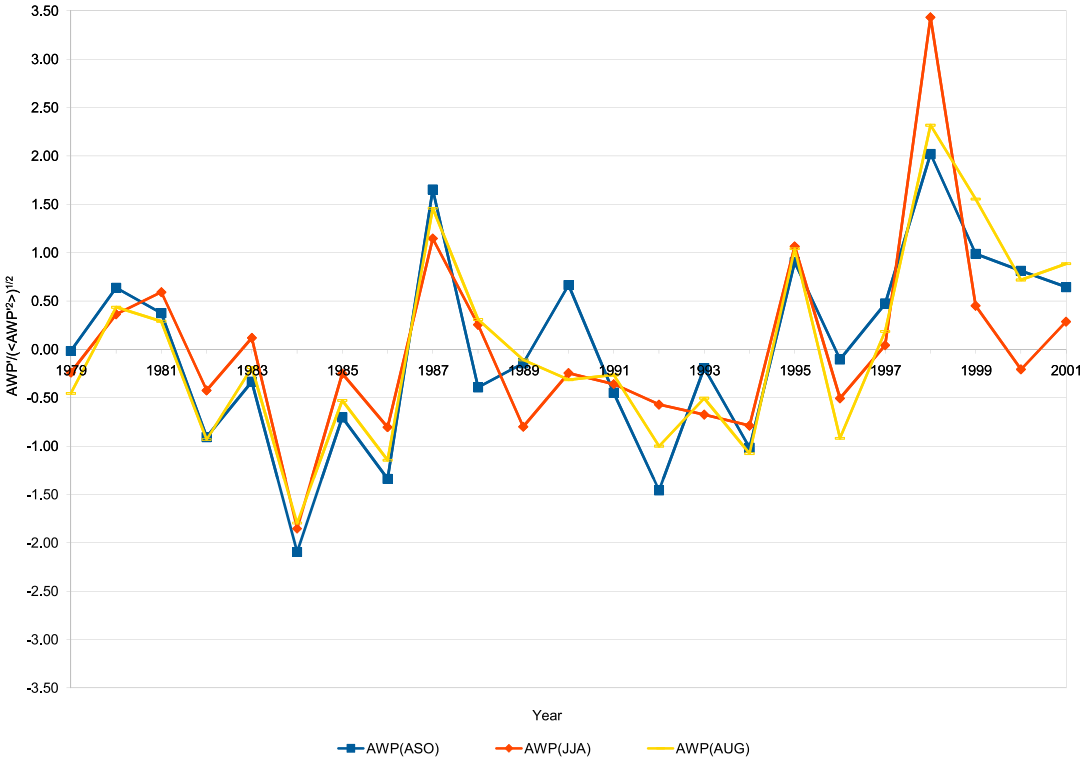

Figure 2. The standard deviation normalized AWP area anomalies between 1979 and 2001. Blue, orange, and yellow lines represent August-September-October (ASO), August, and June-July-August (JJA) anomalies, respectively.

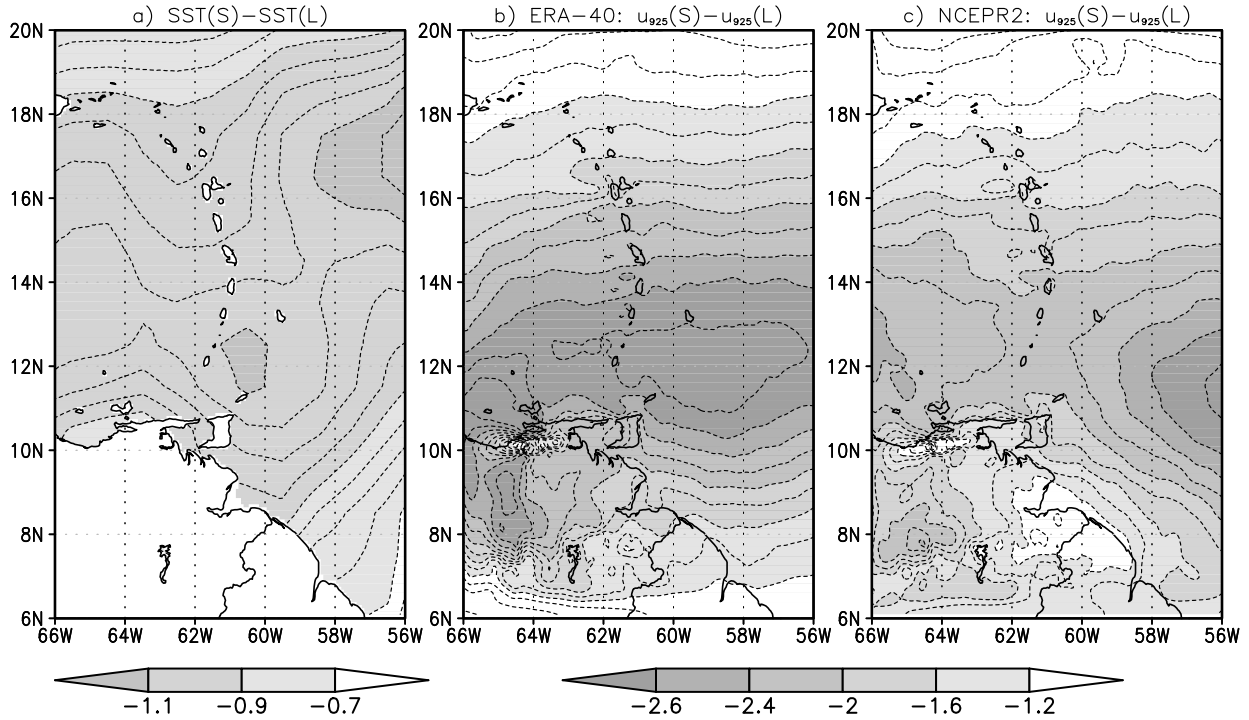

Figure 3. The RSM (a) interpolated SSTs, (b) ERA-40-simulated, and (c) NCEPR2-simulated selected large and small AWP Augusts (small minus large AWP Augusts). Contour intervals are 0.05°C and 0.2 m s^{-1}.

small AWP Augusts. The ERA SST differences decrease both north and south of the Lesser Antilles.

[21] As discussed by *Wang* [2007], the AWP area has a close relationship with the boreal summer CLLJ: stronger (weaker) CLLJs are associated with smaller (larger) AWPs. Shown in Figures 3b and 4 are the differences and composites of reanalyses and RSM-simulated August 925 hPa zonal wind (u_{925}) for the selected large and small AWP Augusts. Reanalyses and their regional simulations generally share similar features. Large AWP Augusts have weaker low-level easterlies across the simulation domain. The easterlies are weaker across the Lesser Antilles; stronger easterlies are evident in the open Atlantic to the east and the CLLJ core to the west.

[22] For the RSM simulations, the island impact on the monthly mean easterlies is clear. RSM-simulated easterlies are weaker in the immediate vicinity and to the west of the islands, and mesoscale easterly maximums are evident between the Lesser Antilles islands (Figure 4). Such features are absent in both global reanalyses, which is not surprising given their coarse model resolutions: NCEP Global Forecast System (GFS) T62 (~180 km), ECMWF ERA-40 T159 (~100 km), and RSM's 8 km horizontal resolution. Terrain-flow interactions in the RSM simulations are evident in northeastern Venezuela. There are enhanced 925 hPa easterlies on the southern flanks of elevated terrain where a LLJ has been observed [*Douglas et al.*, 2005].

[23] Maximum easterlies over the open Atlantic are shifted farther north by about 5° latitude during the large AWP Augusts. The ERA-40 easterlies are generally stronger than the NCEPR2 easterlies for both large and small AWP Augusts. Similar interannual variations and interreanalyses differences are reflected in the corresponding RSM downscaling simulations.

[24] The downscaled and reanalyses easterlies across the islands are not only stronger, but they are also more uniform during the small AWP years. With the exception of Trinidad, 925 hPa easterlies in the RSM simulations and ERA-40 are uniformly 9–9.5 m s^{-1} across all of the Lesser Antilles for small AWP years. For the large AWP RSM simulations, 8+ m s^{-1} easterlies can be found only near the northern end of the Lesser Antilles (Leeward Islands). Over the southern end of the island chain (Windward Islands), 925 hPa easterlies weaken to ~6.5 m s^{-1} during large AWP years.

4. Simulated Lesser Antilles-Surrounding Environment Interactions

4.1. Overview

[25] Changes to regional-scale flow change the climate on the islands, and the islands themselves have their own impact on the regional-scale circulation (as evident in Figure 4). The most obvious impacts of the islands on the regional climate are the introduction of diurnal variability and the increased surface roughness of the island to the otherwise unobstructed easterlies over the open Caribbean Sea. The prescribed RSM Caribbean SSTs are daily averaged. However, the simulated air-sea interface still has diurnal variability due to diurnal varying surface atmospheric conditions and energy budgets.

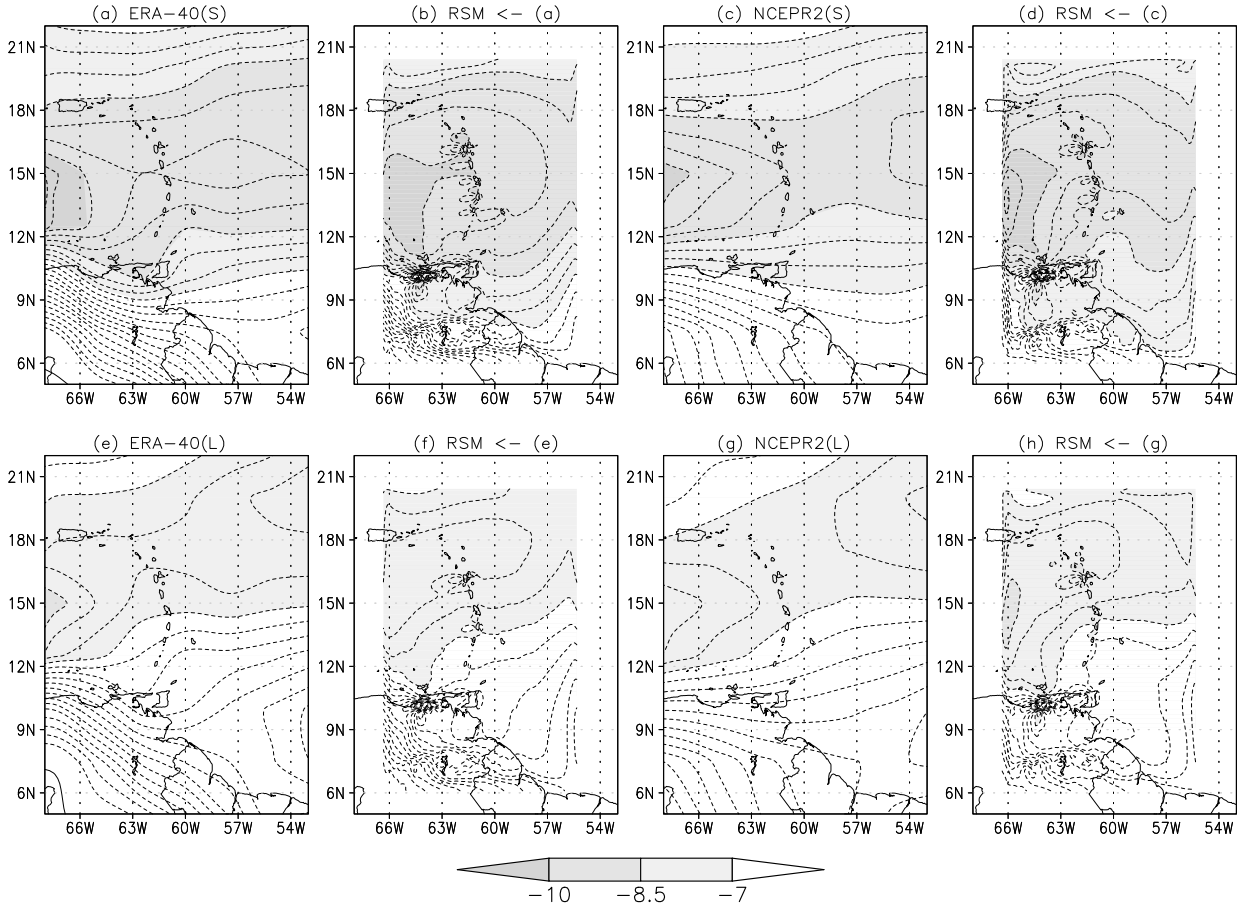

Figure 4. The reanalyses and their RSM downscaled u_{925} for the selected (a, b, c, d) small AWP (1984, 1986, 1994, and 1992) and (e, f, g, h) large AWP (1998, 1999, 1987, and 1995) Augusts. The reanalyses are plotted in Figures 4a, 4c, 4e, and 4g, and their downscalings are in Figures 4b, 4d, 4f, and 4h. Contour intervals are 0.5 m s^{-1}.

For brevity, the discussion here will concentrate on the ERA-40 downscaling.

[26] It is only natural to begin with a discussion that contrasts the diurnal variabilities over the islands with the nearby water. That information is presented in Figure 5: the RSM-simulated diurnal variability of the 2 m temperature (T_{2m}), PBL depth (H_{PBL}), and 10 m wind speed (WS_{10m}). Since it is evident from Figure 4 that there is a distinction between the east (upwind, where the mean flow originates) and the west (downwind, where the mean flow is going) of the islands, our composite in Figure 5 is also further divided into downwind and upwind waters. The island average is normalized by total surface area covered by the islands. In other words, the value is biased toward the large islands.

[27] The simulated diurnal T_{2m} variability over water is much weaker than it is over the islands. During the daytime (nighttime), islands are warmer (colder) than the surrounding waters. Temperatures are highest over the island shortly after noon and are lowest in the dawn hours, with a typical diurnal range of about 5°C. The T_{2m} over water shows signs of a subdiurnal cycle: temperatures are moderately lower (~0.5°C) during the afternoon hours and are highest during the overnight hours and at dawn. The simulated diurnal variability of H_{PBL} is also higher over the islands than over water, consistent with the diurnal variations of T_{2m}.

[28] The composite island nighttime/dawn T_{2m} minimum is slightly higher during the large AWP years (<0.3°C). The early afternoon T_{2m} maximum shows a much larger change (~0.7°C). The simulated island temperature anomalies responding to the surrounding SST anomalies are reflected mostly in the daytime.

[29] The simulated diurnal variations of WS_{10m} over water are consistent with the lower troposphere wind diurnal cycle as analyzed by M08: surface/lower tropospheric winds are strongest overnight and are weakest during the afternoon. Over the islands, WS_{10m} are much lower; wind speeds are about one fourth of the wind speeds over open waters. Curiously, the wind speed is strongest over the islands during the daytime, when the open water wind speeds are lowest. We will discuss this in further detail in section 4.2.

[30] The WS_{10m} (T_{2m}) is lower (higher) on the downwind-leeward side of the islands than on the upwind-windward side, but the difference itself is diurnally varying and is largest during the afternoon. Air that is warmed over the island is

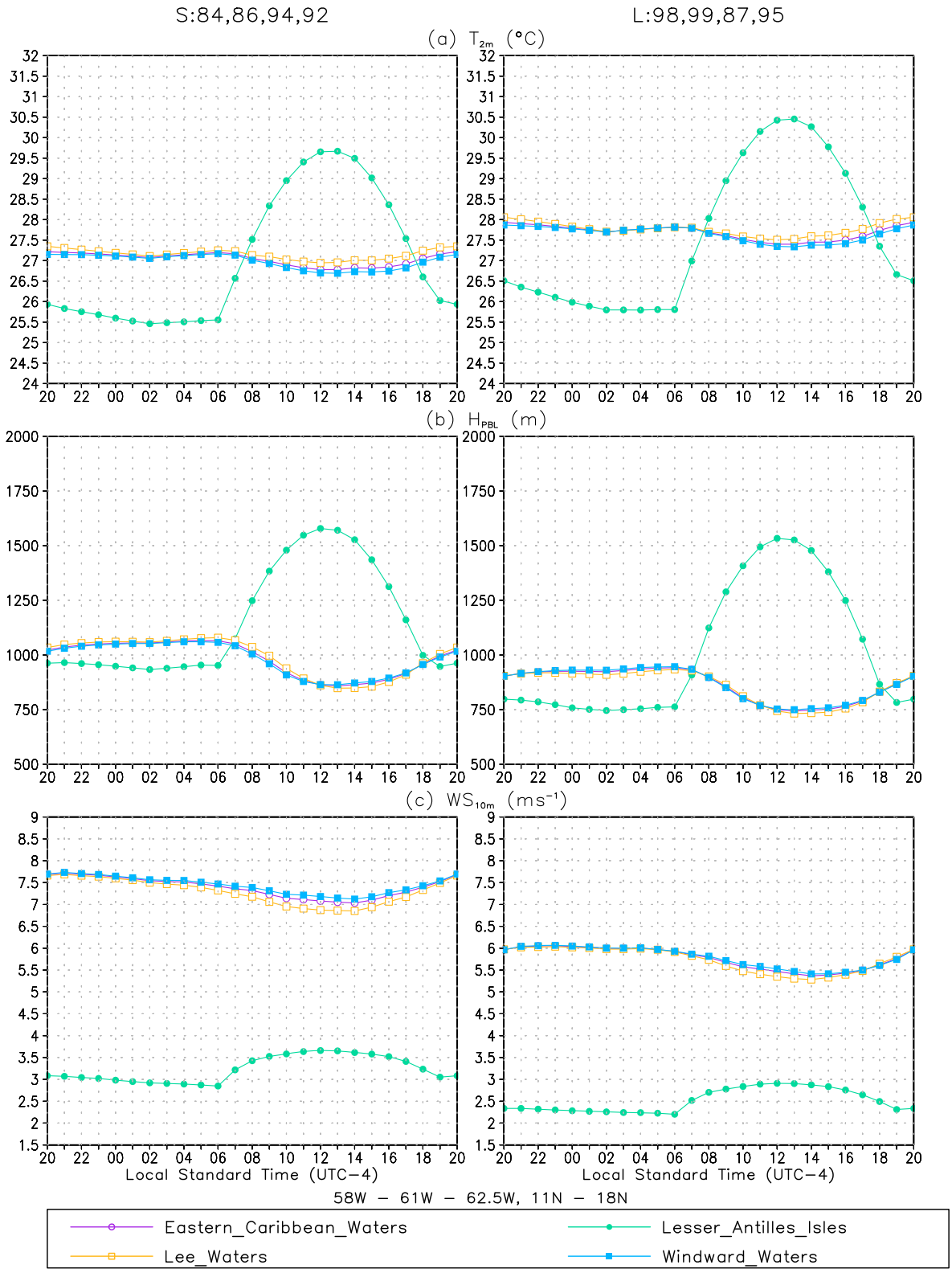

Figure 5. The composite hourly diurnal variability of the (a) 2 m temperature (T_{2m}), (b) PBL depth (H_{PBL}), and (c) 10 m wind speed (WS_{10m}) for all land ("Lesser Antilles Isles") and water points ("East Caribbean Waters") within the box (11°N–18°N, 58°W–62.5°W, Trinidad excluded), and water points that are west (downwind "Lee Waters") and east (upwind "Windward Waters") of 61°W. Above the plots, (left) S denotes small AWP, (right) L denotes large AWP, and numbers denote years.

being advected westward. Therefore, T_{2m} over water west of the islands remains elevated by about 0.1–0.2°C until about 2200 local standard time (LST).

4.2. The Richardson Number Problem

[31] The question is then "How do the islands modulate the climate in the open water around them"? This is fundamentally tied to how the islands can impact the flow surrounding environment. At first order, the problem is essentially a gradient (derivative)/bulk (finite-differencing) Richardson number (Ri) problem. That is, how do the vertically sheared CLLJ easterlies, strongest in the lower troposphere and weakening toward the surface, respond to the islands' diurnal heating?

$$\mathrm{Ri} = \mathrm{Fr}^{-2} = \frac{g}{T_v}\frac{\left(\frac{\partial \theta_v}{\partial z}\right)}{\left(\frac{\partial u}{\partial z}\right)^2 + \left(\frac{\partial v}{\partial z}\right)^2} \approx \frac{g\Delta z}{T_v}\frac{\Delta\theta_v}{\Delta u^2 + \Delta v^2}, \quad (1)$$

where Fr, g, u, v, T_v, and θ_v take on their usual meanings: the Froude Number, the approximate gravitational acceleration near the Earth's surface ($g \approx 9.81\ \mathrm{m\ s^{-2}}$), zonal and meridional wind speeds (u, v), virtual temperature ($T_v \approx T(1 + 0.6q)$), and virtual potential temperature (θ_v). The CLLJ is dominated by the zonal component (M08); however, diurnal variations of the meridional component are significant (CV10). During the daytime, the growth of H_{PBL} over the islands (Figure 5b) leads to vertical mixing of potential temperature, moisture (specific humidity, q), and momentum (which leads to the reduction of the vertical shear).

[32] The impact of the widening of the boundary layer and vertical mixing over the islands is clearly illustrated in Figure 6, where we have plotted the diurnal variability of the vertical differences of q, wind shear, and θ_v between the 1000 hPa and 925 hPa isobars over the islands. The shear between 925 hPa and 1000 hPa isobars is highest during the nighttime and is reduced during the daytime when stronger easterlies mix down toward the surface (Figure 6b) and strengthen the surface wind speeds (as seen in Figure 5c). The opposite applies with moisture: air is drier aloft, and mixing reduces the negative difference (Figure 6a).

[33] The reduction of wind shear between 925 hPa and 1000 hPa is associated with a reduction of average wind speed of the lower troposphere. Shown in Figure 7a is the average wind speed (WS) between 925 hPa and 1000 hPa. The average WS is lowest during the daytime (~0.5 m s^{-1} less than the nighttime/dawn maximum) as kinetic energy of the mean flow is lost to turbulent kinetic energy (TKE) through diurnal vertical mixing [*Holton*, 2004].

[34] Considerable PBL variations are observed between the different islands. Some of the individual islands stand out: the small islands have weaker diurnal variations, and Trinidad has a distinctly large variation. All the one-grid-point islands (Nevis, Barbuda, and Montserrat; boldface in Table 1) and some of the smaller islands (Marie Galante and Antigua) have weaker diurnal variability in the vertical wind shear and θ_v differences.

[35] The one-grid-point islands, Marie Galante, and Antigua have T_{2m} diurnal variabilities that are comparable to those of the other islands. In Figure 8, we have shown the diurnal variability of the same three variables used in Figure 5 over the individual islands. With the exception of Trinidad, T_{2m} varies between 26°C and 30°C. The three one-grid-point islands stand out in terms of the daily average WS_{10m}, which is higher by about 0.5 m s^{-1} compared to that of all other "bigger" islands. Unlike the WS_{10m} of the one-grid-point islands, the WS_{10m} of Marie Galante and Antigua is generally comparable to that of the other Lesser Antilles islands (except Trinidad).

[36] Trinidad's diurnal mean and variability are particularly notable. Trinidad is not only the largest of the islands, but it's location, close to the South American coast with far less open water downwind to the west, is unique. Because of its geographical location and its relatively large size among the other Lesser Antilles islands, Trinidad warrants a study specifically focusing on it alone.

[37] Unlike Trinidad, the one-grid-point islands are crowded toward the northern end of the Lesser Antilles and are the farthest away from the South American coast. We will discuss the location of the one-grid-point islands in detail in section 5 under interannual variability, especially in comparison with Antigua, a "larger" island that is in proximity to the three one-grid-point islands.

[38] The other islands between Trinidad and the one-grid-point islands have varying degrees of diurnal variability in the 925 hPa and 1000 hPa vertical difference of T_v, θ_v, q. Using Figure 8 as a reference, we have plotted u_{925} at the time H_{PBL} are deepest (~1400 local time) and shallowest (~0500 local time) in Figure 9. The local 1400 local time u_{925} is characterized by alternating stronger easterlies between and behind the islands and weaker easterlies in front of (windward side) and behind (leeward side) the islands, a classic signature of lee waves. The feature is simulated regardless of whether the AWP is anomalously large or small. The feature is absent at the northern end of the islands near the one-grid-point islands. At 0500 local time (Figures 9b and 9d), the easterlies are stronger over the open water, and lee wave features are actually less prominent. Easterlies remain relatively weak upwind of the islands in large AWP years as compared to the small AWP years.

[39] Equation (1) tells us how the island modifies the mean flow when it crosses over the islands. During the daytime, wind speeds increase near the land surface, and vertical shear is reduced as island thermals mix momentum downward. If the islands are "flat," the diurnal cycle of lower troposphere is controlled only by the diurnal thermals (Ri increases). For "hilly" islands, increased terrain interaction leads to increased mechanical turbulence and gravity waves (Ri decreases).

[40] The diurnal variations of thickness (Δz) and average T_v between 925 hPa and 1000 hPa isobars are small (Figures 7b and 7c).

$$\frac{T_{v,\mathrm{day}} - T_{v,\mathrm{night}}}{\overline{T}_v}, \frac{\Delta z_{v,\mathrm{day}} - \Delta z_{v,\mathrm{night}}}{\overline{\Delta z}} \ll 0.01, \quad (2)$$

$$\overline{\Delta z} \approx \Delta z_{\mathrm{day}} \approx \Delta z_{\mathrm{night}}, \quad (3)$$

$$\overline{T}_v \approx T_{v,\mathrm{day}} \approx T_{v,\mathrm{night}}. \quad (4)$$

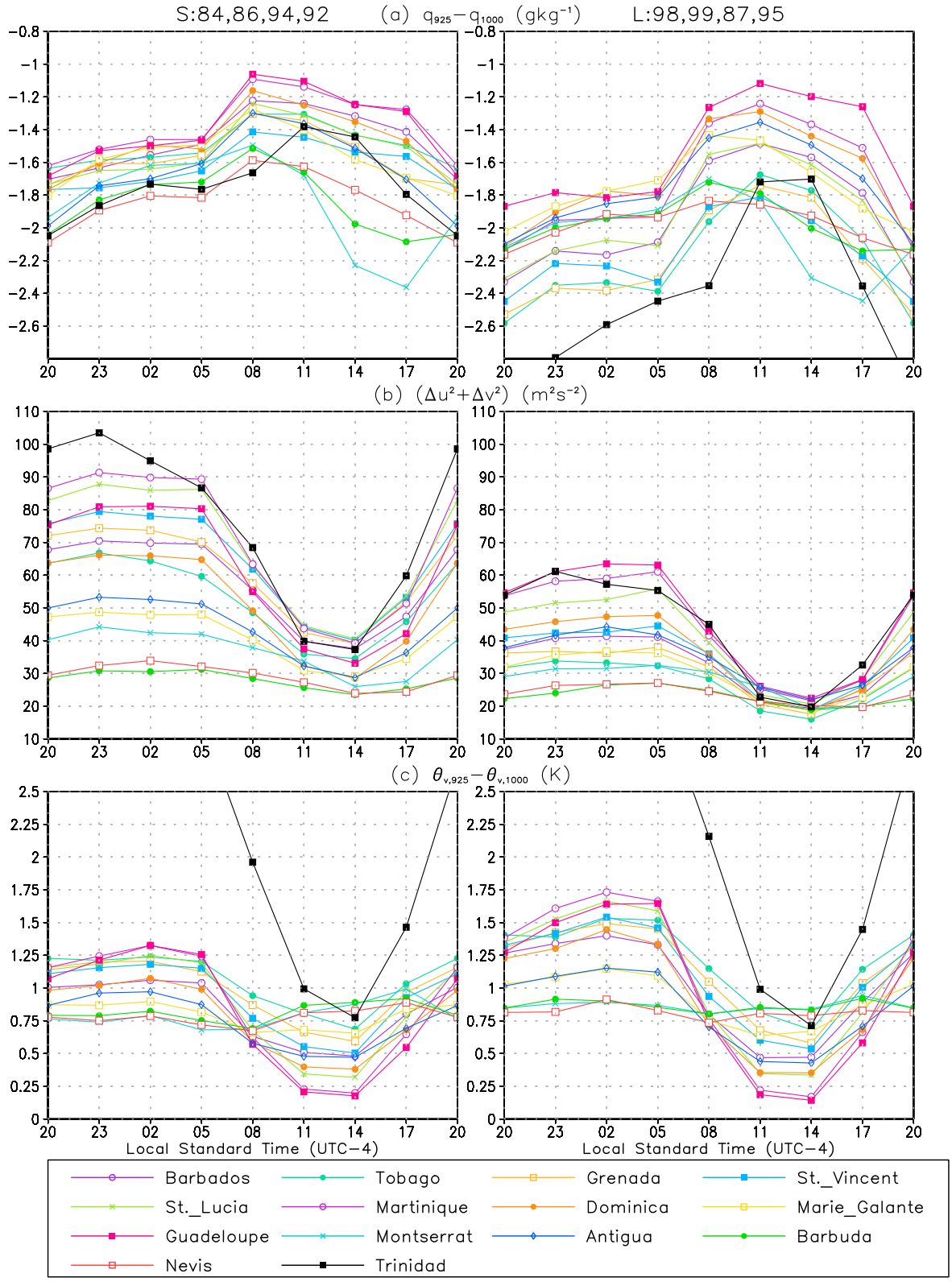

Figure 6. Similar to Figure 5 but for the different islands (labeled) and the difference of (a) specific humidity (q_{925}-q_{1000}), (b) wind shear (squared) $(u_{925} - u_{1000})^2 + (v_{925} - v_{1000})^2$, and (c) virtual potential temperature ($\theta_{v,925}$-$\theta_{v,925}$) between 925 hPa and 1000 hPa isobars.

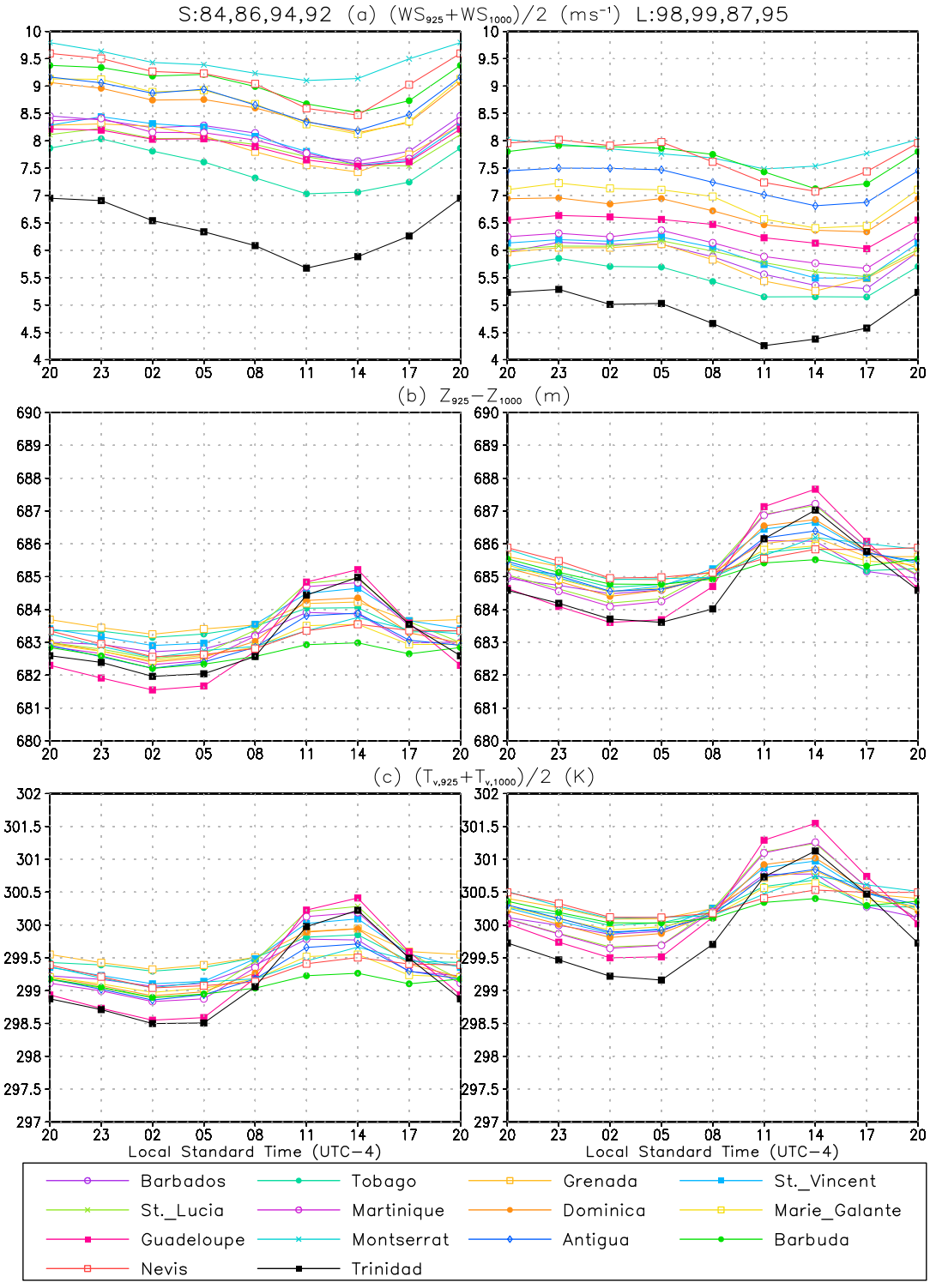

Figure 7. Same as in Figure 6 but for the 925 hPa and 1000 hPa average WS ($1/2(WS_{925}+WS_{1000})$), average T_v ($1/2(T_{v,925}+T_{v,1000})$), and the difference of 925 hPa and 1000 hPa geopotential height ("thickness," Z_{925}-Z_{1000}).

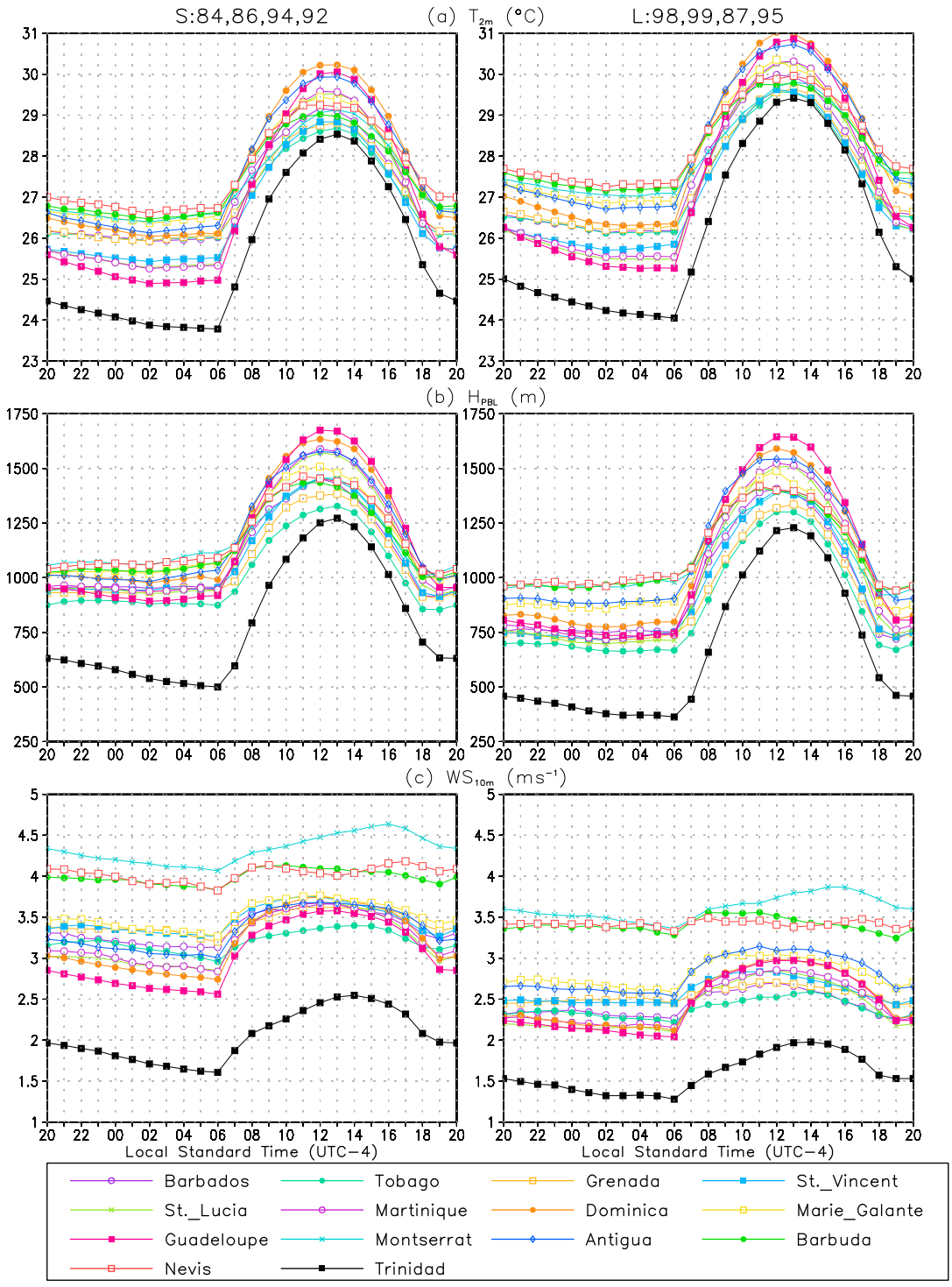

Figure 8. Similar to Figure 6 but for the diurnal variability for the ERA-40 downscaled (a) T_{2m}, (b) H_{PBL}, and (c) WS_{10m} over the resolved individual Lesser Antilles isles.

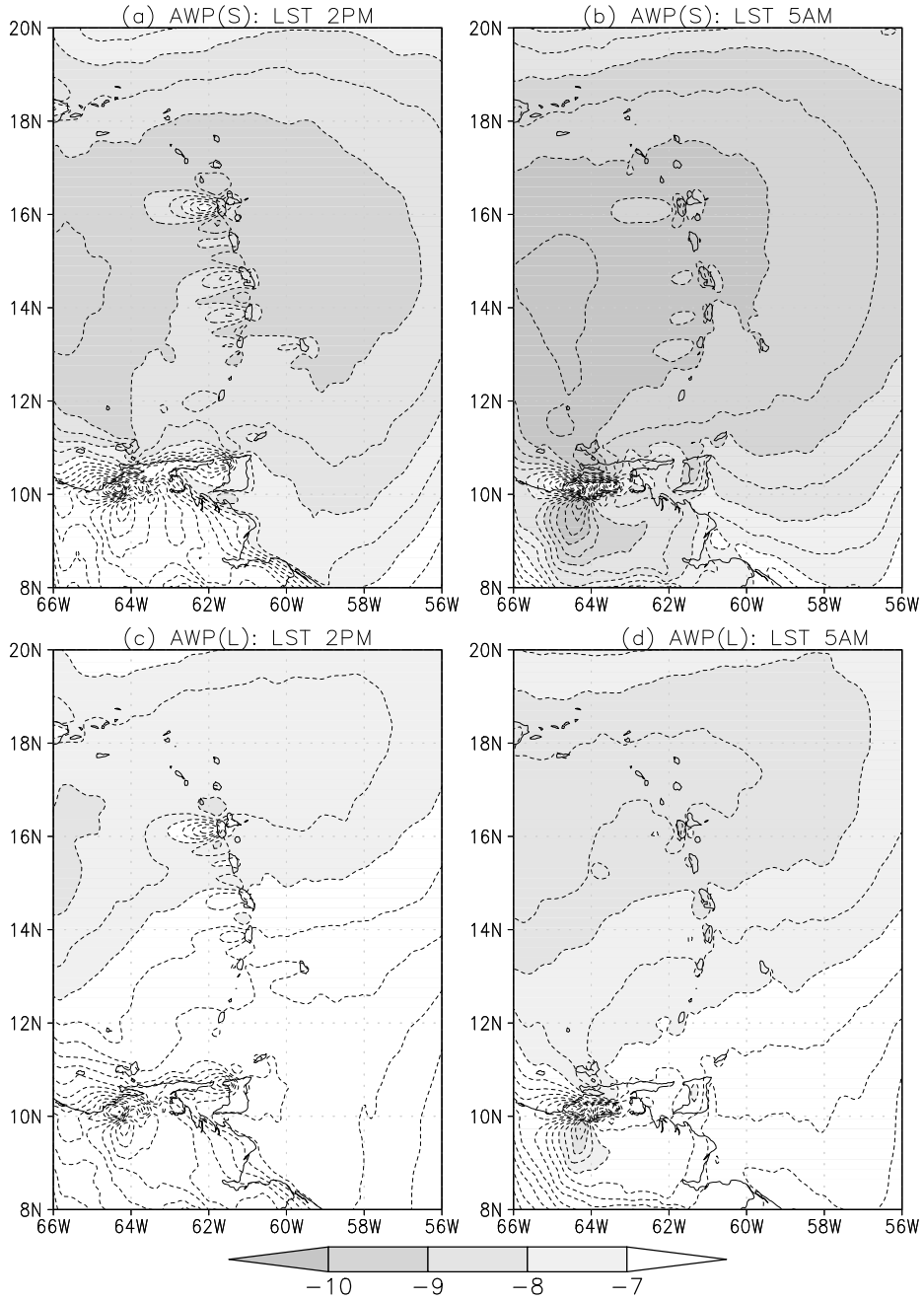

Figure 9. The (a, b) small and (c, d) large AWP composite u_{925} at (left) 1400 local standard time (1800 UT) and (right) 0500 local standard time (0900 UT) over the eastern Caribbean. Contour intervals are 0.5 m s^{-1}.

The Richardson number diurnal variations become diurnal variations of the vertical shear (squared) and θ_v differences in the lower troposphere.

$$\frac{\mathrm{Ri}_{day}}{\mathrm{Ri}_{night}} \approx \left(\frac{\Delta\theta_{v,day}}{\Delta\theta_{v,night}}\right)\left(\frac{\Delta u_{night}^2 + \Delta v_{night}^2}{\Delta u_{day}^2 + \Delta v_{day}^2}\right) = \left(\frac{\Delta\theta_{v,day}}{\Delta\theta_{v,night}}\right)\left(\frac{S_{day}}{S_{night}}\right)^{-1} \tag{5}$$

$$S = \Delta u^2 + \Delta v^2 = (u_{1000} - u_{925})^2 + (v_{1000} - v_{925})^2, \tag{6}$$

where S is the shear term. The diurnal variations of S, $\Delta\theta_v$, and Ri of the individual islands are shown in Table 4.

[41] Ri decreases during the daytime for larger and hillier islands. For smaller islands, Ri increases during the daytime. The hilly islands (such as Guadeloupe and Martinique) have especially low values in the third and sixth columns of Table 4. Terrain heating leads to higher θ_v on the 1000 hPa isobar through elevated sensible heating. This is the same as saying a smaller $\Delta\theta_v$ and a stronger reduction of reduced gravity (the Brunt-Väisälä frequency), and that drives Ri down. For the smaller islands with poorly resolved topographic

Table 4. Diurnal Variations (Fractional) of 925 hPa and 1000 hPa Vertical Wind Shear (S), θ_v, and Bulk Richardson Number of the Lesser Antilles[a]

	Small AWP			Large AWP		
Island	$\frac{S_{day}}{S_{night}}$	$\frac{\Delta\theta_{v,day}}{\Delta\theta_{v,night}}$	$\frac{\mathrm{Ri}_{day}}{\mathrm{Ri}_{night}}$	$\frac{S_{day}}{S_{night}}$	$\frac{\Delta\theta_{v,day}}{\Delta\theta_{v,night}}$	$\frac{\mathrm{Ri}_{day}}{\mathrm{Ri}_{night}}$
Barbados	0.539	0.453	0.840	0.468	0.337	0.721
Tobago	0.536	0.554	1.033	0.481	0.448	0.931
Grenada	0.530	0.492	0.928	0.486	0.389	0.800
St. Vincent	0.513	0.426	0.829	0.441	0.348	0.788
St. Lucia	*0.472*	*0.254*	*0.539*	*0.394*	*0.202*	*0.512*
Martinique	*0.437*	*0.150*	*0.344*	*0.367*	*0.098*	*0.266*
Dominica	*0.432*	*0.354*	*0.818*	*0.397*	*0.244*	*0.614*
M. Galante	0.608	0.730	1.201	0.510	0.584	1.146
Guadeloupe	*0.408*	*0.134*	*0.327*	*0.354*	*0.087*	*0.247*
Montserrat	**0.612**	**1.112**	**1.816**	**0.610**	**0.942**	**1.544**
Antigua	0.546	0.485	0.888	0.497	0.372	0.748
Barbuda	**0.769**	**1.080**	**1.404**	**0.710**	**0.923**	**1.300**
Nevis	**0.705**	**1.048**	**1.488**	**0.757**	**0.864**	**1.141**
Trinidad	*0.393*	*0.255*	*0.650*	*0.346*	*0.218*	*0.631*

[a]See equations (5) and (6). Islands that occupy only one grid point and 10+ grid points are in boldface and italics, respectively. Antigua is noted for its unique interannual variability (see section 5).

features, the islands act as hot spots with their surface terrain comparatively unimportant. In Table 4, sixth column values are systematically lower than those of the third column. This difference is related to the preferential sensitivity of daytime temperatures to AWP anomalies (see section 5).

[42] Despite the increased mechanical-generated turbulence for the larger and hillier islands during the daytime, the increase of mechanical lee waves is still fundamentally connected with heating-induced reduction of vertical stability. The above results also show that the modeled island-atmosphere interaction is sensitive to the model-resolved island size and topography.

4.3. Why Do "Antilles-less" Reanalyses Have Wind Minimums Near the Islands?

[43] The impact of islands on the easterlies across the eastern Caribbean is explicitly resolved by RSM model dynamics. However, global reanalyses cannot resolve the impact of an island without actually having the island resolved within the assimilating model. The validity of Figure 4 is then called into question: there are 925 hPa easterly minimums in the vicinity of the Lesser Antilles in both ERA-40 and NCEPR2 reanalyses. Upper air observations from the Lesser Antilles are assimilated into both reanalyses even though the islands do not exist in the assimilating model [*Uppala et al.*, 2005; J. Wollen, NCEP, personal communications, 2010]. Further analysis of this feature is beyond the purview of this paper. However, the above discussion highlights the value of producing high-resolution regional reanalysis, in which the true impacts of the island are explicitly resolved.

5. The Relationship With AWP Variability and Island Diurnal Variability

[44] In section 4, we focused on the islands' impacts on the regional climate. In section 5, we revisit Figures 3 through 8 to focus on how changes of AWP are reflected on the islands.

[45] As shown in section 4, the simulated interannual variability of the island's diurnal variability is dependent on the size of the island. AWP variability can influence the island's climate by modulating tropical cyclone activities [*Wang and Lee*, 2007]. For the eight selected Augusts, only one tropical storm/hurricane entered our domain (TS Arthur, 1984) [*Lawrence and Clark*, 1985]. In this paper, however, changes in tropical cyclone (and other synoptic) variability will not be discussed. We will focus on diurnal variability as we did in section 4.

[46] Because of our experimental design (prescribed daily mean SST) and the lack of diurnal variability over the ocean, the AWP interannual variability of T_{2m} and winds over water is most pronounced in the shift of the daily average (Figure 5). Over the islands, both daily maximum and minimum T_{2m} are increased during the large AWP Augusts; however, the change of daily T_{2m} maximum at interannual scales is clearly larger than the daily T_{2m} minimum (Figure 5a).

[47] The composite diurnal variability of T_{2m}, H_{PBL}, and WS_{10m} is shown in Figure 8 for the ERA-40 downscaled integrations. This information is also summarized in Tables 5 and 6 where we present the differences of diurnal minimum, maximum, and average T_{2m} between the large and small AWP years. Table 6 shows the average both in terms of island land area average (Island (per island land area); same as in Figure 5, equation (7)), and as an island average (Island (per island), equation (8)):

$$\overline{T_{2m(i)}} = \frac{\sum_{n=1}^{N} a_n T_{2m,n}}{\sum_{n=1}^{N} a_n}; N = \#\text{ island grid points} \tag{7}$$

$$\overline{T_{2m(ii)}} = \frac{1}{M}\sum_{m=1}^{M}\left(\frac{\sum_{l=1}^{L_m} a_l T_{2m,l}}{\sum_{l=1}^{L_m} a_l}\right); M = \#\text{ islands},$$
$$L_m = \#\text{grid points on island } m, \tag{8}$$

where a is the area of grid point as referred by the subscript (n and l).

[48] In agreement with the results shown in Figure 5, the interannual variability of the daily T_{2m} maximum over all individual islands is larger than the interannual variability of the daily T_{2m} minimum. The average change between large and small AWP (Table 6, tenth, eleventh, and twelfth columns) of the maximum, minimum, and daily average T_{2m} over the islands, however, is approximately the same regardless of whether this averaging is performed per area or per island. But the actual values of the maximum and minimum T_{2m} are dependent on the averaging method. Averaging per island reduces diurnal temperature range ΔT_{2m} (fourth and eighth columns in Table 5). The interannual variability of daily average T_{2m} over the islands is smaller than the simulated values over water. The T_{2m} variability over water itself is weaker than the variability of the prescribed diurnally invariant daily average SST. The prescribed SST differences between large and small AWP Augusts are at least 0.9°C around the Lesser Antilles (see Figure 3).

Table 5. The Simulated Daily Maximum (T_{max2m}), Daily Minimum (T_{min2m}), Daily Range (ΔT_{2m}), Daily Average T_{2m} (°C), and Their Differences for the Islands During Small and Large AWP Augusts[a]

Island	Small AWP				Large AWP				Difference Between Small and Large AWP		
	T_{max2m}	T_{min2m}	ΔT_{2m}	$\overline{T}_{2m}$	T_{max2m}	T_{min2m}	ΔT_{2m}	$\overline{T}_{2m}$	T_{max2m}	T_{min2m}	$\overline{T}_{2m}$
Barbados	29.2	25.9	3.3	27.1	30.0	26.1	3.9	27.6	0.8	0.2	0.5
Tobago	28.7	25.9	2.8	26.9	29.6	26.1	3.5	27.4	0.9	0.2	0.5
Grenada	28.8	25.9	2.9	27.0	29.6	26.2	3.4	27.5	0.8	0.3	0.5
St. Vincent	28.8	25.4	3.4	26.7	29.6	25.7	3.9	27.1	0.8	0.3	0.4
St. Lucia	*29.5*	*25.3*	*4.2*	*26.9*	*30.3*	*25.5*	*4.8*	*27.3*	*0.8*	*0.2*	*0.4*
Martinique	*29.6*	*25.3*	*4.3*	*26.9*	*30.3*	*25.5*	*4.8*	*27.4*	*0.7*	*0.2*	*0.5*
Dominica	*30.2*	*26.0*	*4.2*	*27.6*	*31.0*	*26.3*	*4.7*	*28.1*	*0.8*	*0.3*	*0.5*
M. Galante	29.4	26.4	3.0	27.5	30.4	26.8	3.6	28.1	1.0	0.4	0.6
Guadeloupe	*30.0*	*24.9*	*5.1*	*26.9*	*30.9*	*25.3*	*5.6*	*27.5*	*0.9*	*0.4*	*0.6*
Montserrat	**29.1**	**26.4**	**2.7**	**27.4**	**29.8**	**27.0**	**2.8**	**28.0**	**0.7**	**0.6**	**0.6**
Antigua	29.9	26.1	3.8	27.6	30.7	26.7	4.0	28.3	0.8	0.6	0.7
Barbuda	**29.0**	**26.5**	**2.5**	**27.5**	**29.8**	**27.2**	**2.6**	**28.2**	**0.8**	**0.7**	**0.7**
Nevis	**29.2**	**26.6**	**2.6**	**27.7**	**30.0**	**27.2**	**2.8**	**28.3**	**0.8**	**0.6**	**0.6**
Trinidad	*28.5*	*23.8*	*4.7*	*25.6*	*29.4*	*24.0*	*5.4*	*26.2*	*0.9*	*0.2*	*0.6*

[a]Islands that occupy only one grid point and 10+ grid points are in boldface and italics, respectively. Antigua is noted for its unique interannual variability (see section 5).

[49] The reason averaging by islands leads to a smaller diurnal temperature range is illustrated in Table 5. For most (not all) islands, the change in minimum daily temperature is less than half of the change in daily maximum temperature. But all one-grid-point islands and Antigua have daily minimum temperature changes that are twice as large as the changes for the rest of the islands. Marie Galante, whose PBL diurnal variation shares similarities with that of the one-grid-point islands and Antigua, has a large versus small AWP T_{2m} difference that resembles that of the larger islands. The change of daily average T_{2m} for all the one-grid-point islands and Antigua is, therefore, a consequence of the changes in the daily mean T_{2m} from the interannual variations of the AWP. For the other islands, including all islands that are represented by more than 10 grid points, the change due to AWP variations comes largely from the changes in daily T_{2m} maximum.

[50] The simulation results over the one-grid-point islands are consistent with the results from section 4.1. The small islands display diurnal T_{2m} variabilities comparable to those of the large islands, but the small islands are unable to modify local wind circulations. Therefore, as far as the low-level winds are concerned, the islands do not exist. However, why does Antigua behave the same way as the one-grid-point islands? The location of Antigua further complicates the problem as the one-grid-point islands and Antigua are all in the same vicinity, in the northern end of the Lesser Antilles, where the interannual variations of the low-level easterlies due to AWP variations are relatively weak (see Figure 3).

6. Precipitation Changes and Sensitivities to Forcing Reanalyses

[51] The discussion so far has focused on temperature and lower tropospheric winds. As for the actual local impacts, precipitation is of higher importance than both temperature and lower tropospheric winds. The relationship between Caribbean rainfall anomalies and AWP variability is well understood [*Wang*, 2007]. The precipitation differences between the large and small AWP Augusts may not be very surprising; naturally, warmer SST (larger AWP) will lead to increased precipitation. What may be of more interest are the differences between the reanalyses and the sensitivity of the RSM simulation to the forcing reanalyses.

[52] The height of Central America midsummer drought occurs during August, but such drought is not as evident in the eastern Caribbean [*Magaña et al.*, 1999; *Amador*, 2008]. The composite August RSM and reanalyses precipitations are shown in Figure 10. As a comparison, CMAP and TRMM precipitation analyses are shown in Figure 11. As expected, rainfall is decreased for the small AWP Augusts (Figures 10a–10d) for both reanalyses and RSM simulations; the differences between the large and small AWP simulations

Table 6. The Average Simulated Daily Maximum (T_{max2m}), Daily Minimum (T_{min2m}), Daily Range (ΔT_{2m}), Daily Average T_{2m} (°C), and Their Differences Over All Islands and Water Grid Points Within the Box (11.0°N–18.0°N and 58.0°W–62.5°W) for Small and Large AWP Augusts[a]

Terrain	Small AWP				Large AWP				Difference Between Small and Large AWP		
	T_{max2m}	T_{min2m}	T_{max2m}	T_{max2m}	T_{max2m}	T_{min2m}	ΔT_{2m}	$\overline{T}_{2m}$	T_{max2m}	T_{min2m}	$\overline{T}_{2m}$
Islands (per island land area)	29.7	25.5	4.2	27.0	30.5	25.8	4.7	27.6	0.8	0.3	0.6
Islands (per island)	29.3	25.9	3.5	27.2	30.2	26.3	3.9	27.8	0.9	0.4	0.6
Water	27.2	26.8	0.4	27.0	27.9	27.4	0.5	27.7	0.7	0.6	0.7

[a]The island averages are computed both in terms of per island land area (Trinidad excluded; weighting in favor of the larger islands) and per island. See equations (7) and (8). The box is the same box as in Figure 5.

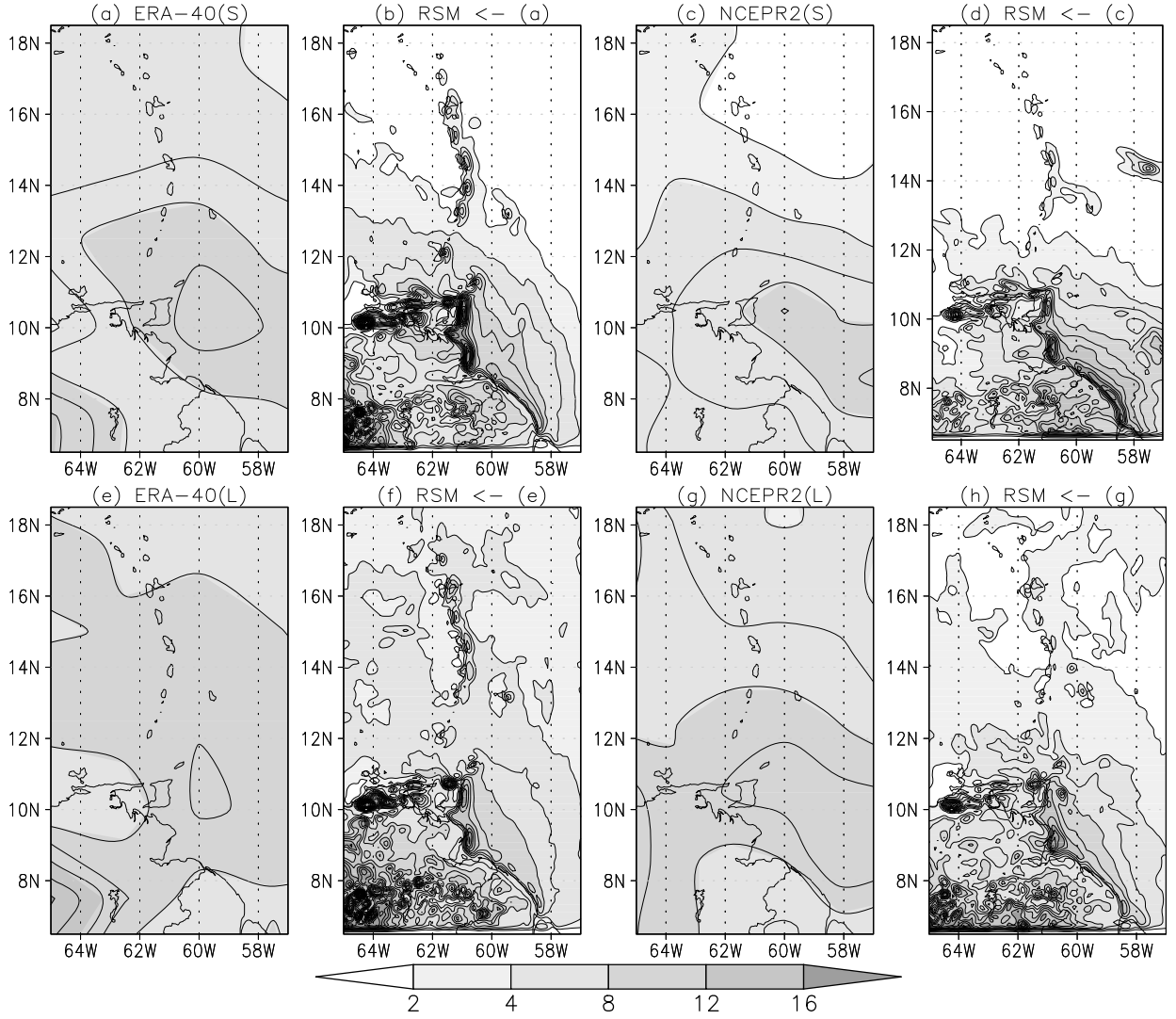

Figure 10. The ERA-40 reforecasted, NCEPR2 reforecasted, and RSM-simulated precipitation for the selected (a, b, c, d) small and (e, f, g, h) large AWP Augusts. Contour intervals are 2 mm d^{-1}.

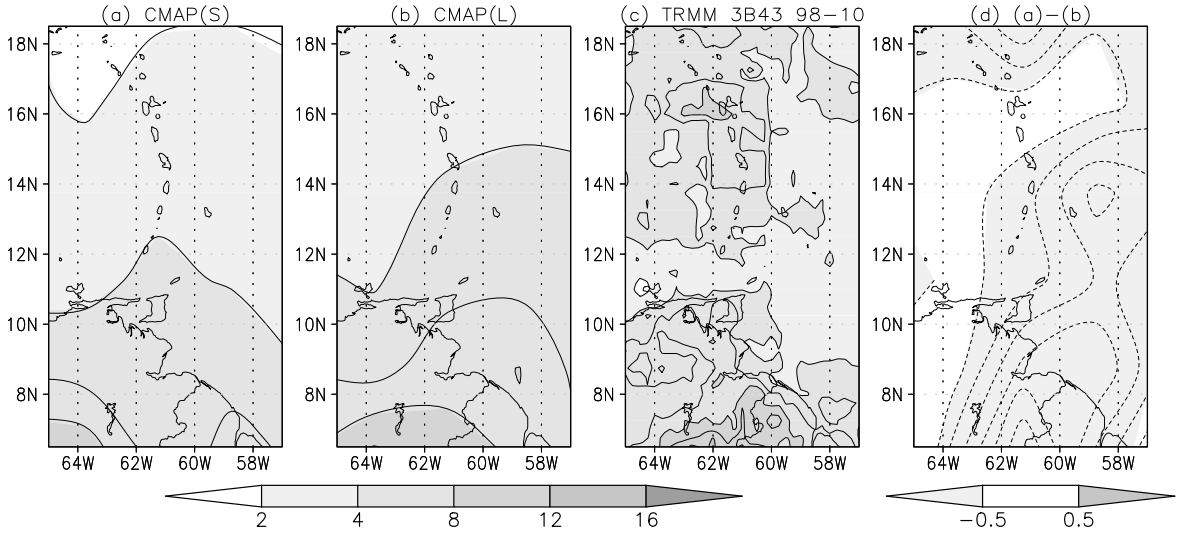

Figure 11. Same as in Figure 10 but for (a, b) CMAP and (c) merged TRMM precipitation analysis. Figures 11a and 11b show CMAP precipitation for the selected small and large AWP Augusts, and Figure 11c shows TRMM 1998–2010 August averages. (d) CMAP differences; contour intervals are 0.5 mm d^{-1}.

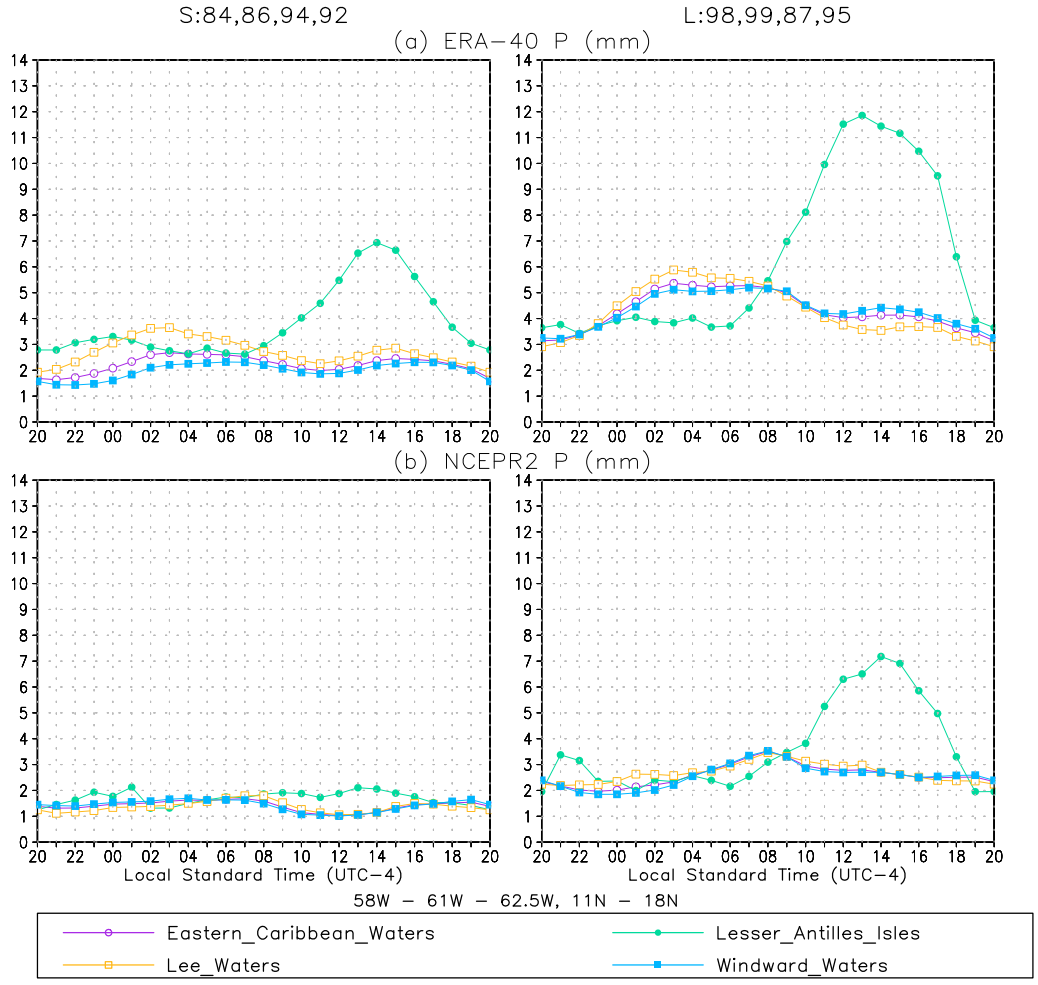

Figure 12. Same as in Figure 5 but for (a) ERA-40 downscaling precipitation and (b) NCEPR2 downscaled precipitation. Units are in mm d^{-1}.

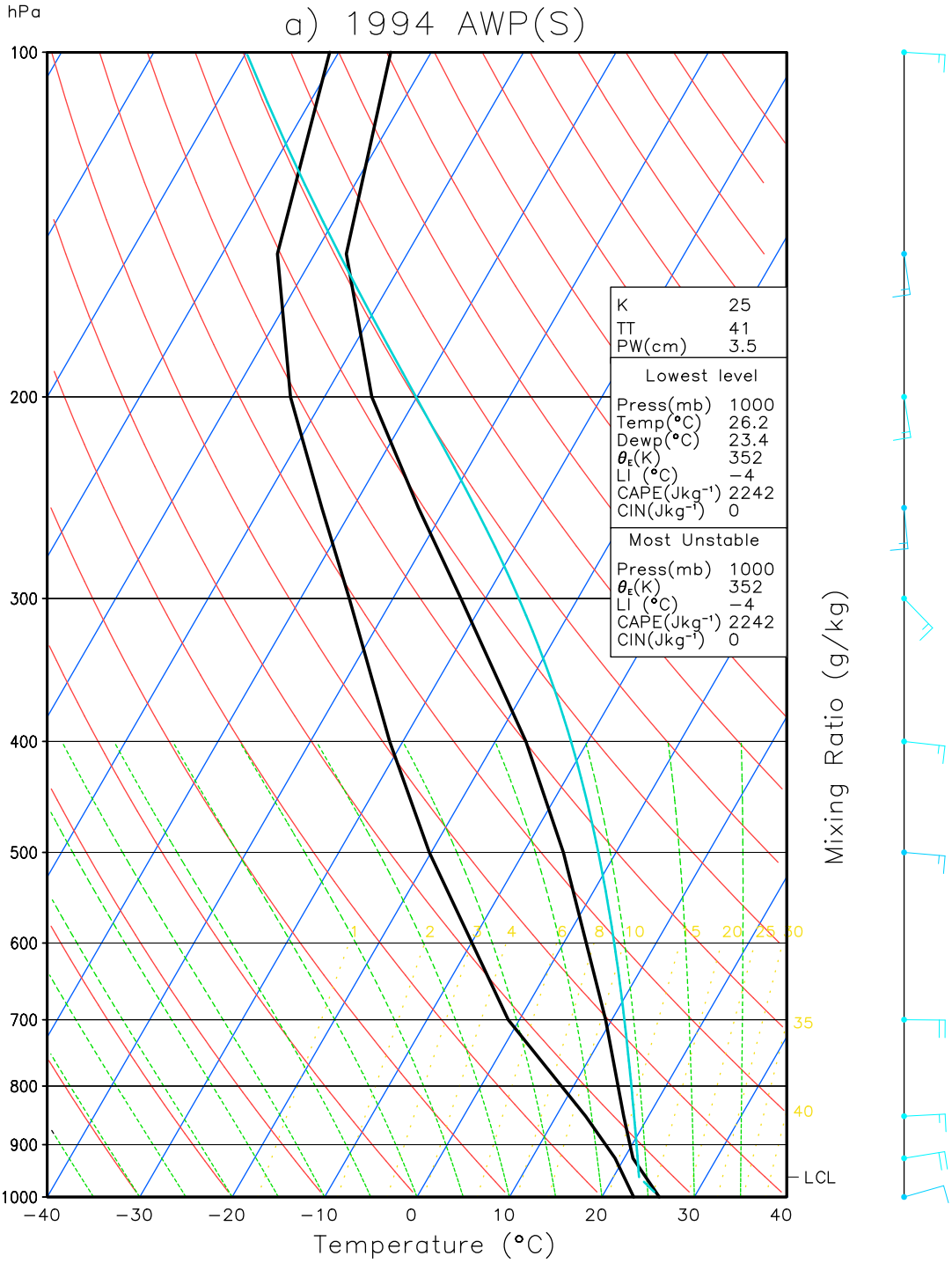

Figure 13. (a) Observed and (b) RSM-simulated upper atmosphere soundings over Barbados for August 1994.

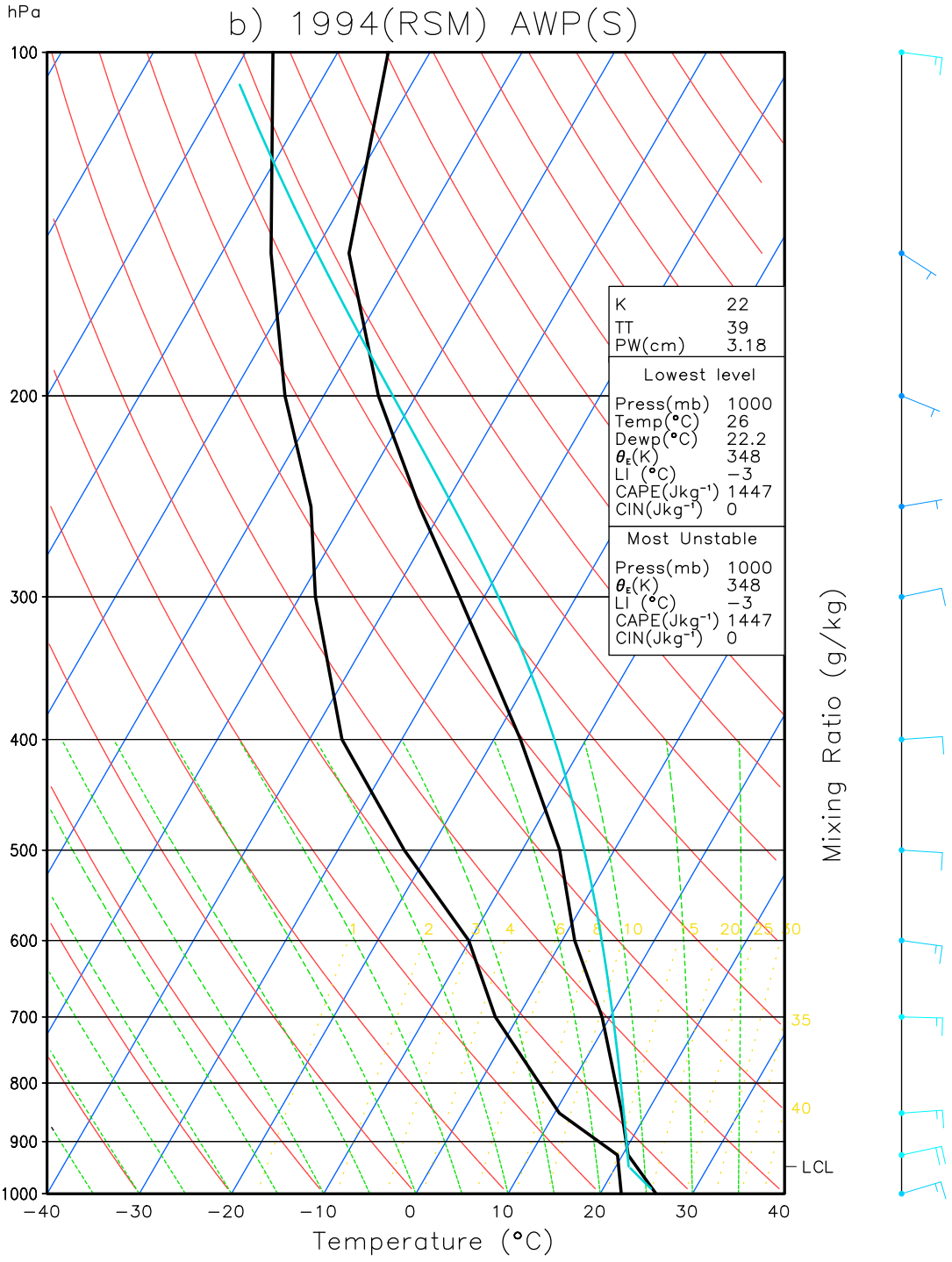

Figure 13. (continued)

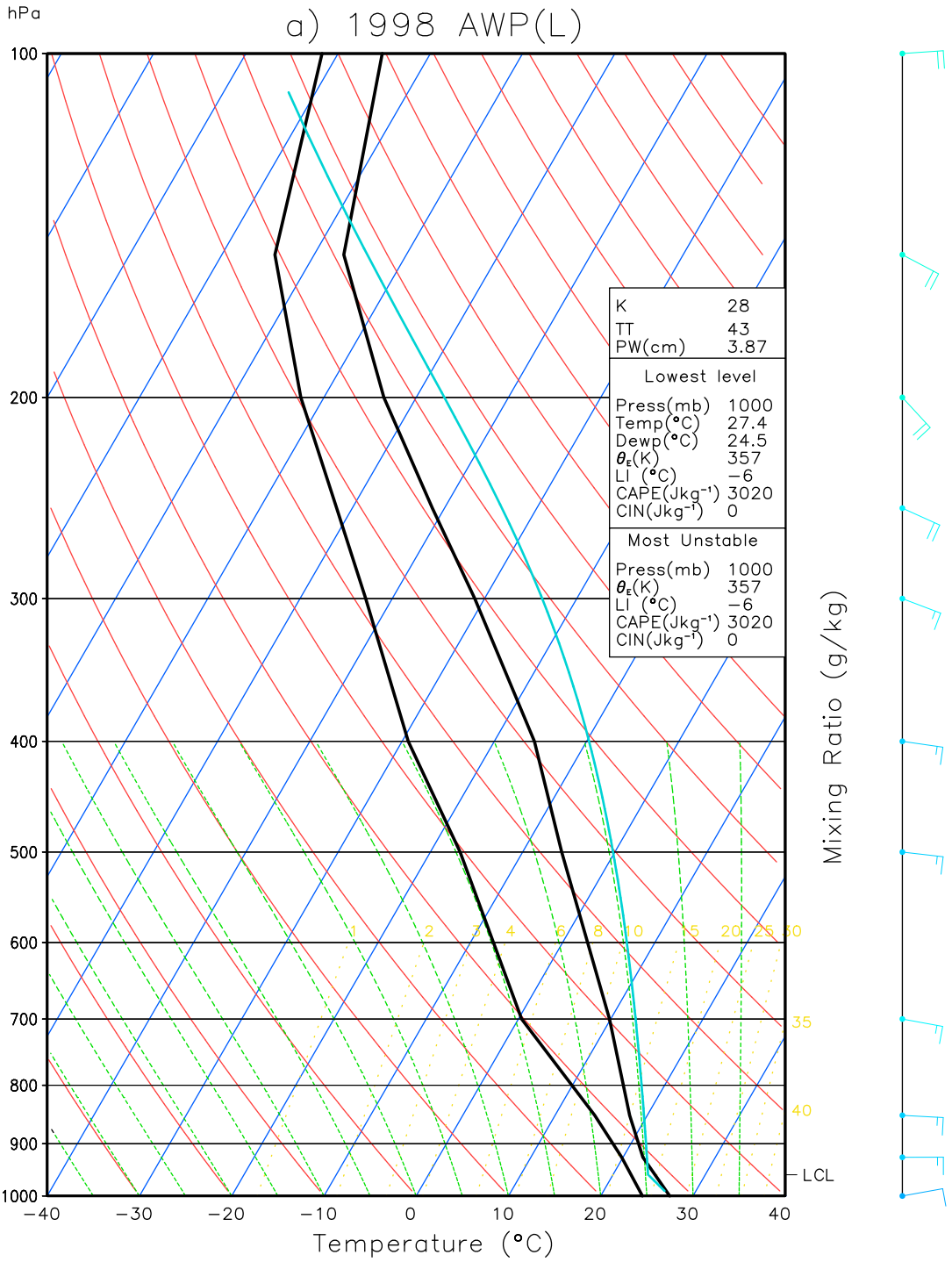

Figure 14. Same as in Figure 13 but for 1998.

are most noticeable for the Leeward Islands. CMAP analysis shows a similar precipitation decrease, with the bulk of the decrease to the east of the Lesser Antilles.

[53] For the RSM simulations, "bull's eyes" in precipitation line up along the islands. Because of the coarse resolution of the CMAP analysis, it is not possible to distinguish such island maximums (Figures 11a and 11b). For TRMM analysis (Figure 11c), there are hints that such maximums exist. Over open waters, RSM downscaled simulations have less precipitation than their original forcing reanalysis. Precipitation in ERA-40 has a tendency to be higher than NCEPR2 precipitation, and the downscaled simulations follow the same pattern. To summarize the differences, we have plotted the differences between the islands and water in Figure 12 in the

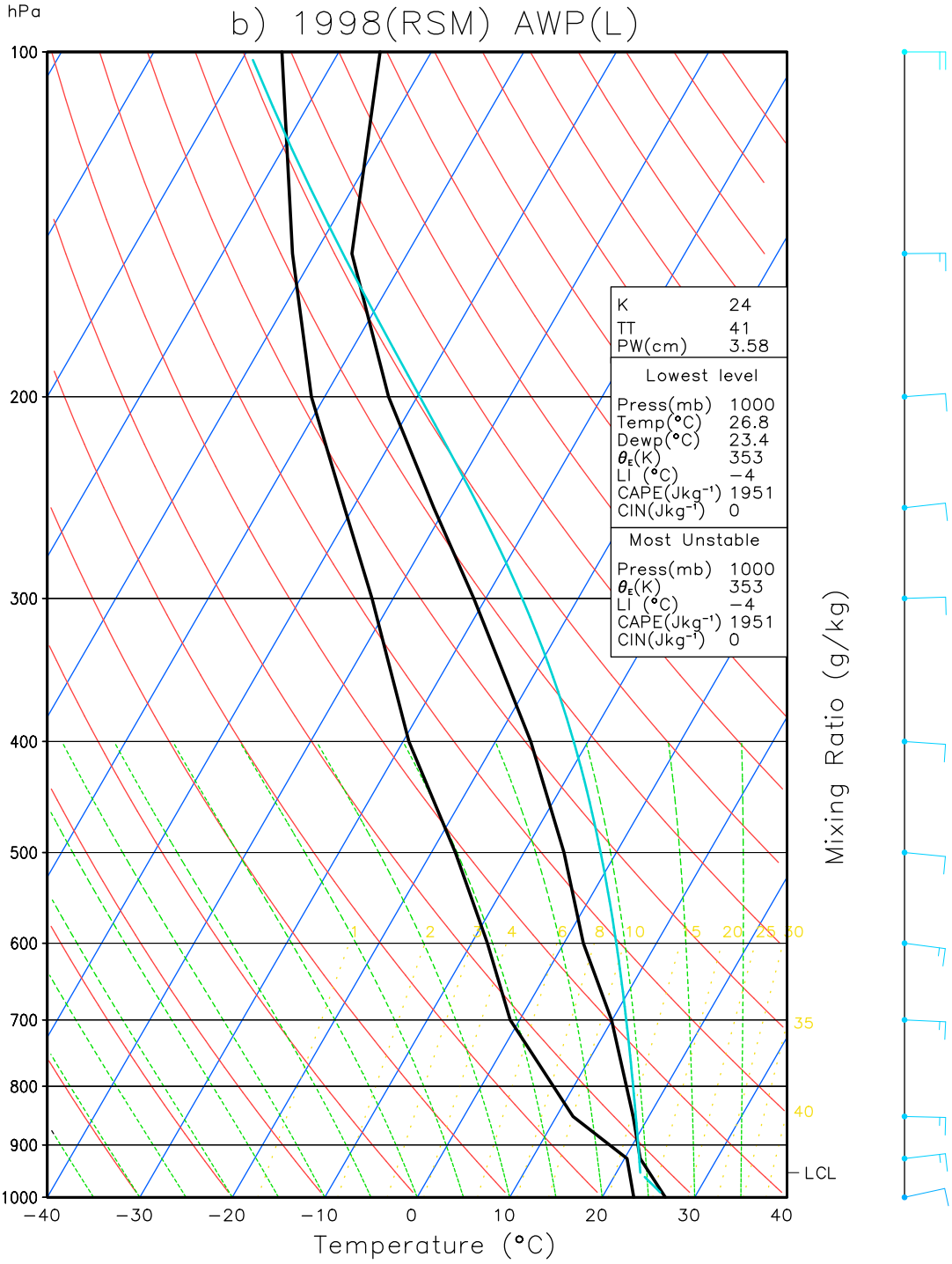

Figure 14. (continued)

same manner used in Figure 5. In the NCEPR2 simulations, the "increased" midday precipitation over the islands for small AWP years is so small that it is only one third of the small AWP ERA-40 simulations.

[54] A more convectively and wet ERA-40 tropical and equatorial Atlantic relative to NCEP/NCAR reanalysis is mentioned by *Uppala et al.*, [2005] and *Chan and Nigam* [2009]. Because of the similarity between NCEPR2 and the NCEP/NCAR reanalysis assimilating model, the differences here between ERA-40 and NCEPR2 are not surprising. Regardless, compared to CMAP, both reanalyses overestimate the actual rainfall for both warm and small AWP

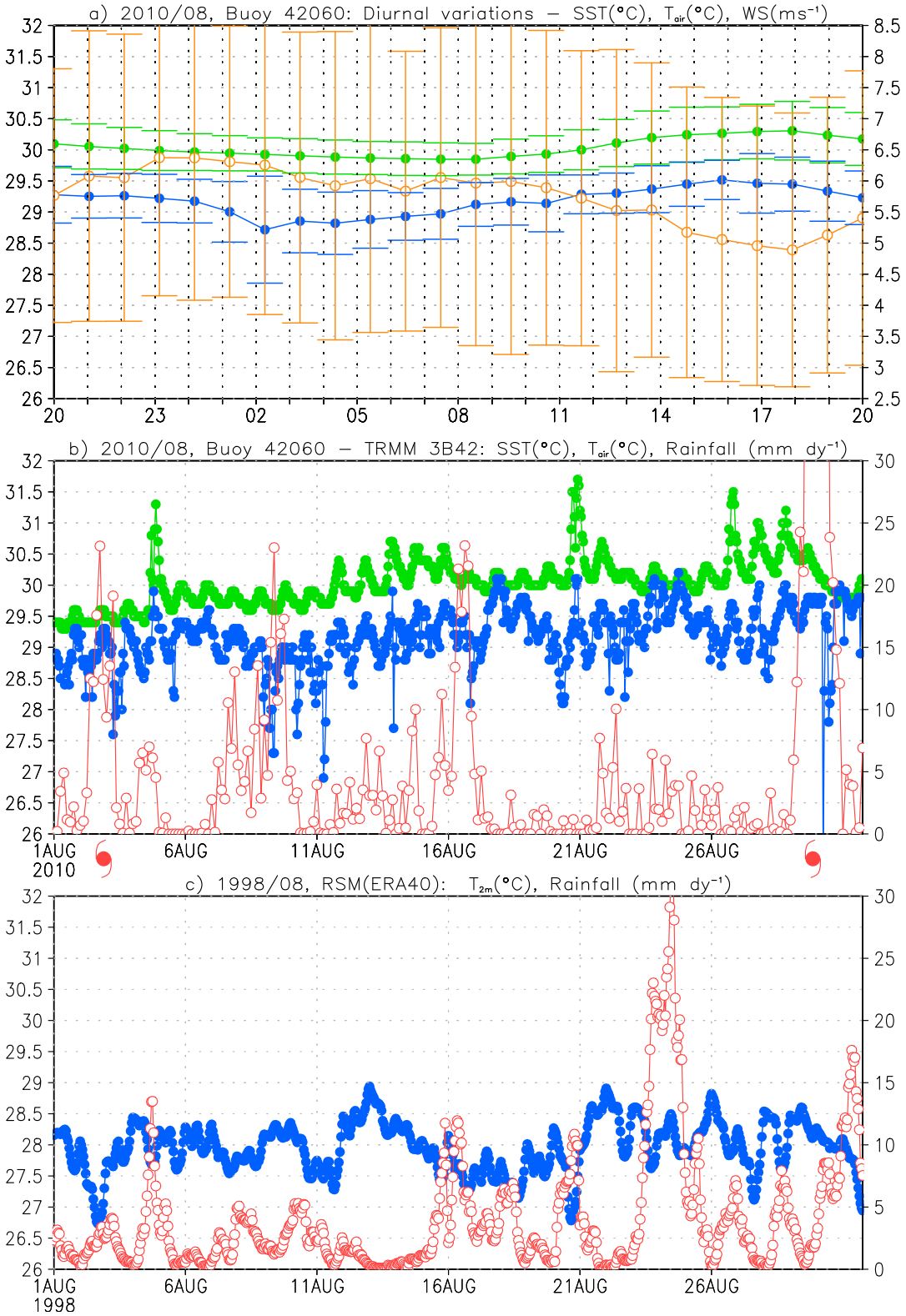

Figure 15. (a) The diurnal variability (in local time) of surface air temperature (blue), wind speed (orange), and SST (green) as observed by NBDC NOMAD buoy 42060 for August 2010. (b) The buoy hourly surface air temperature (blue), SST (green), and box-averaged 3-hourly 3B42 TRMM precipitation (see text). Passing tropical systems (TS Danielle and Hurricane Earl) are marked. (c) As a comparison, RSM-simulated marine (islands excluded) T_{2m} and precipitation for August 1998 are shown.

Augusts. A reduction of the rainfall in the RSM simulations over the Lesser Antilles and the open waters is an improvement over the original reanalyses.

7. In Situ Observations

7.1. In Situ Upper Air Observations

[55] Twice-a-day (2300–0000 UT/1900–2000 local time and 1100–1200 UT/0700–0800 local time) vertical soundings are available from Barbados Grantley Adams International Airport for the period between 1965 and 2007 [*Durre et al.*, 2006]. Because of the sounder launch times, the data are unsuitable for any day versus night comparisons. However, quantitative comparisons can be made between large and small AWP years.

[56] Because of the unavailability of 925 hPa-level upper air observations from earlier years, here we compare 2 years from the 1990s (1994 and 1998). The time-averaged August observed and RSM-simulated vertical soundings from Barbados for those two years are shown in Figures 13a, 13b and 14a, 14b. The features of the soundings are generally consistent with the discussions in sections 3, 4, and 6. Both soundings indicate a moist and well-mixed boundary layer. High relative humidity is evident at 925 hPa. Above 925 hPa, there is a rapid decrease of dew point with height and reduced lapse rate. That hints at the existence of inversion-capped boundary layer clouds.

[57] The large 1998 AWP has a more unstable troposphere (higher CAPE) than the 1994 AWP, consistent with the difference of rainfall between the large and small AWP Augusts. RSM-simulated CAPE is lower than the soundings, but both sounding and simulated CAPE values are high (1000+ J kg^{-1}), suggesting an unstable troposphere.

7.2. In Situ Ocean Observations

[58] We obtained buoy observations for the Caribbean from the National Data Buoy Center (NDBC) [*Hamilton*, 1986]. Buoy 42060 (16.5°N, 63.5°W; marked in Figure 1) is located approximately 150 km west of Montserrat. However, "historical" hourly data are available only after 2009, so direct comparisons with our model simulations are not possible.

[59] Shown in Figures 15a and 15b are the diurnal averages and hourly August 2010 observations from buoy 42060. To illustrate synoptic variability, 11°N–18°N 58°W–62.5°W box-averaged (same box used in Figure 5) TRMM 3B42 rainfall analyses over the eastern Caribbean are plotted as well. Buoy 42060s diurnal air temperature range is ~0.4°C, comparable to the RSM-simulated values (see Figure 5). However, there are differences in the diurnal phase, with observed air temperature tending to peak at dusk hours.

[60] Buoy-measured surface wind speeds tend to show a high degree of variability with the standard deviation on the same order of the hourly diurnal average value. Buoy wind speeds tend to be at a minimum during late afternoon and dusk hours. RSM-simulated surface wind speed minimums tend to occur 2–3 h earlier at around 1400–1500 local time (Figure 5b).

[61] Temperature variations (+1°C) associated with lower-frequency synoptic variability are much larger than diurnal variability. Cooler buoy air temperature can be seen after notable rainfall events. As a quantitative comparison, Figure 15b is reproduced for 1998 for the RSM simulation (Figure 15c). Synoptic variations dominate the RSM-simulated precipitation variability for the region. Both Figures 15b and 15c imply a 1–10 day returning period of synoptic rainfall events, consistent with observed Atlantic easterly wave variabilities [*Reed et al.*, 1977]. A realistic representation of periodicity of rainfall events is hardly unexpected, as the simulations are forced by reanalyses. However, the apparent relationship between surface air temperature and rainfall is not evident.

8. Discussions and Conclusions

[62] In this paper, we have discussed how the Lesser Antilles climate is modulated by the AWP variability and how the islands themselves are modulating the marine climate of the eastern Caribbean. The simulated interactions between the islands and the regional climate are diurnally varying as a consequence of the diurnal heating of the islands. Island interactions are strongest during the daytime as the islands warm and their boundary layer expands.

[63] AWP SST anomalies can be communicated to the islands only through the atmosphere. The island's diurnal air temperature variability is much higher than that of the surrounding water, and the simulated maximum air temperatures over the island differ greatly from the marine environment that surrounds it. Therefore, it is natural to ask how the AWP anomalies manifest in the islands. For surface temperatures on the "larger" islands (islands greater than 10 grid points), the manifestation appears only during the daytime. During the nighttime, the decoupled boundary layers and land breezes keep the islands essentially isolated. The island must be large or hilly enough to modulate the mesoscale atmospheric circulations around it, as shown in Figure 9. For all one-grid-point (smallest resolvable) islands, the island is just too small to interact with the prevailing low-level easterlies, and the temperature anomalies over the islands, day or night, largely reflect the anomalies of the SST around the islands.

[64] The peculiarity of Antigua's changes of maximum and minimum temperature raises the question of whether Antigua's location and shape have played a role. In light of the existence of islands similar to Antigua in area size and Richardson number diurnal variation (such as St. Vincent and Barbados), results here suggest that Antigua's location may have played a role. A prerequisite for a detailed study for the above problem is a dynamical model that can resolve the coastlines of the smaller islands. RSM is unsuitable for such a high-resolution modeling study because the model is not designed for nonhydrostatic dynamics and cloud-resolving physics.

[65] CV10 have pointed out the importance of thermally forced pressure gradients in forcing diurnal variations of the CLLJ. In Figure 16, we show the meridional mean T_{2m} across our domain at 0500 1400 local time; the island chain introduces a ~0.2°–0.4°C perturbation against the background zonal negative temperature gradient. At noon, the zonal gradients of temperature to the west of the islands are weakened as a result of the island. The warmed islands should lead to a lower tropospheric trough to the east of CLLJ core. Following the arguments by M08 and CV10, the zonal temperature gradients would introduce a geostrophic northerly wind component to the CLLJ. However, the flow behind the

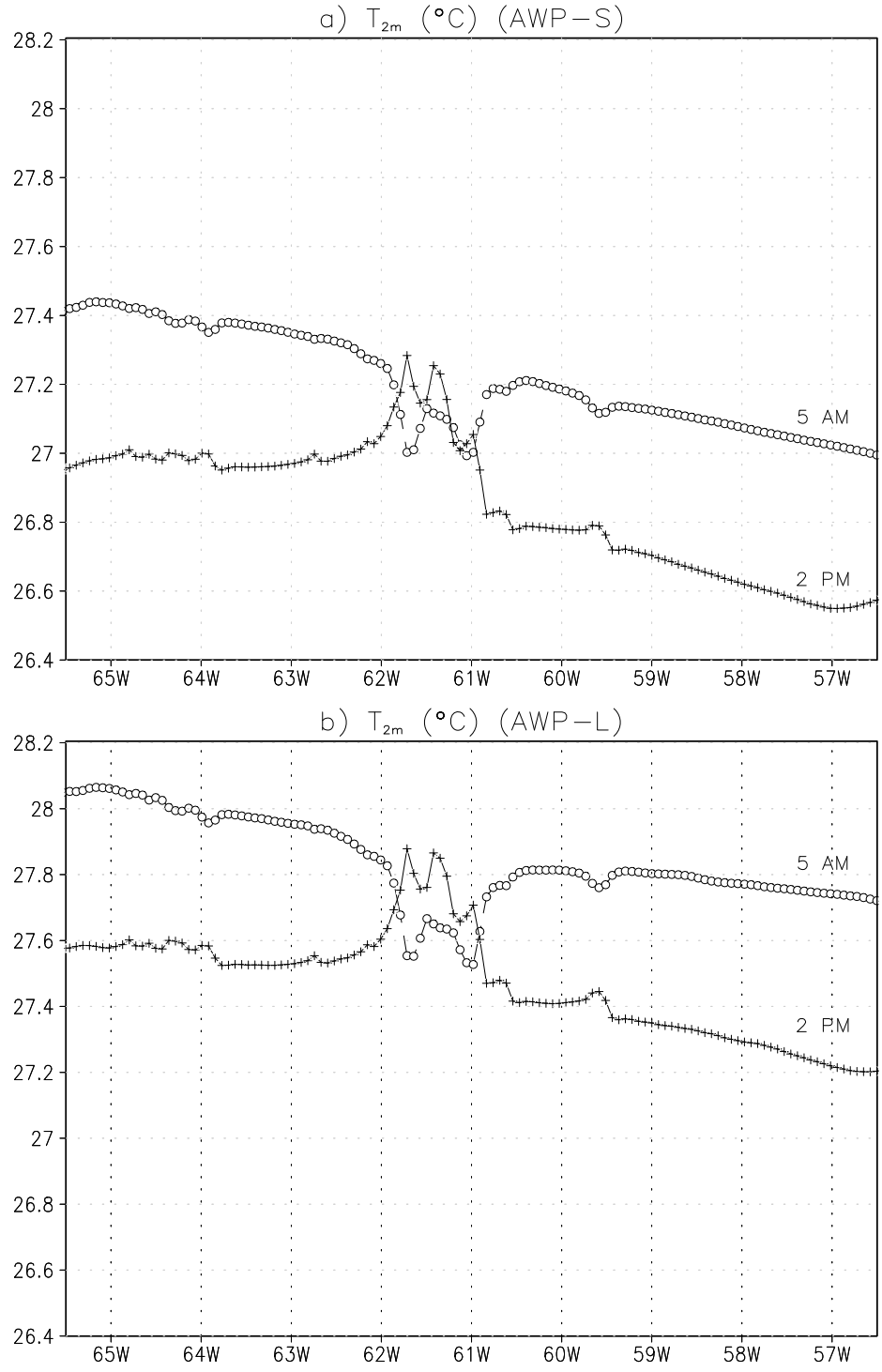

Figure 16. The average T_{2m} between the latitude 11°N–18°N for the (a) small and (b) large AWP. Circles and pluses are for 0500 local time (0900 UT) and 1400 local time (1800 UT), respectively. No land masking has been used.

Lesser Antilles actually turns southerly during the daytime (not shown). Instead, the work here highlights the importance of the frictional (PBL) effects as described in CV10. Since low-level flow is approximately zonal, diurnal variations of island drag would have the most impact in the zonal wind diurnal variations. The diagnosed zonal frictional acceleration in CV10 is large (see CV10, Figure 5). Results here show a need to examine the frictional term more carefully. Section 4.3 suggests island drag is built into the coarse-grid global reanalyses through data assimilation. However, the

following two open-ended CLLJ questions remain unanswered: (1) What if the island upper air observations are not assimilated into the coarse-grid reanalyses? Would there still be an easterly minimum over the Lesser Antilles? (2) How would the Atlantic easterlies and CLLJ respond if the Lesser Antilles and South American coastal mountains are removed?

[66] Analyses of in situ observations show considerable challenge in simulating the diurnal variations of near-surface marine climate. The magnitude of the marine air-temperature diurnal variability is reasonably simulated, but the phase appears to be erroneous when compared with limited (1 month) buoy observations. There is also no clear evident subdiurnal cycle in the buoy observation, and the model is unable to simulate the observed T_{2m} reduction during rainfall events. Is this tied to the prescription of daily averaged SST? The observed precipitation-T_{2m} relationship suggests the importance of cloud cover, which is controlled by the model's cumulus and radiation schemes.

[67] We have discussed the forcing reanalyses representation of the eastern Caribbean climate and the value added by dynamically downscaling them. The simulation shows features that are basically nonresolvable by the coarser-grid model and reduces the reanalysis rainfall biases in the region. It is encouraging to note that downscaling from a reanalyses that has poor (excessive) Caribbean rainfall (ERA-40) does not lead to a poor downscaled precipitation. Comparisons between simulated and observed gridded island precipitation are handicapped by the coarse resolution of the gridding. The work presented here, which is mostly based on model simulations, indicates a need to improve in situ observations. Observations must be obtained for the calmer, "less interesting" overnight hours to gain a better understanding of the diurnal variability. Possibilities for future research include using in situ radar measurements.

[68] **Acknowledgments.** We thank the SIO Experimental Climate Prediction Center for sharing RSM with us. We would also like to thank Jack Wollen of NOAA for providing information about radiosonde inputs used in reanalyses. We would also like to thank Kathy Fearon of FSU COAPS for providing editorial assistance in preparing this manuscript. Computational resources are provided by FSU High Performance Computing. The project described in this publication was supported by grant/cooperative agreement 06HQGR0125 from the United States Geological Survey and U01 EH000421 from the Center for Disease Control. Its contents are solely the responsibility of the authors and do not necessarily represent the official views of the U.S. Geological Survey and the Center for Disease Control.

References

Amador, J. A. (2008), The intra-Americas sea low-level jet, *Ann. N. Y. Acad. Sci.*, *1146*(1), 153–188, doi:10.1196/annals.1446.012.

Bosilovich, M. G., and S. D. Schubert (2002), Water vapor tracers as diagnostics of the regional hydrologic cycle, *J. Hydrometeorol.*, *3*(2), 149–165, doi:10.1175/1525-7541(2002)003<0149:WVTADO>2.0.CO;2.

Carbone, R. E., J. W. Wilson, T. D. Keenan, and J. M. Hacker (2000), Tropical island convection in the absence of significant topography. Part I: Life cycle of diurnally forced convection, *Mon. Weather Rev.*, *128*(10), 3459–3480, doi:10.1175/1520-0493(2000)128<3459:TICITA>2.0.CO;2.

Chan, S. C., and S. Nigam (2009), Residual diagnosis of diabatic heating from ERA-40 and NCEP reanalyses: Intercomparisons with TRMM, *J. Clim.*, *22*(2), 414–428, doi:10.1175/2008JCLI2417.1.

Cook, K. H., and E. K. Vizy (2010), Hydrodynamics of the Caribbean low-level jet and its relationship to precipitation, *J. Clim.*, *23*(6), 1477–1494, doi:10.1175/2009JCLI3210.1.

Douglas, M. W., J. Murillo, and J. Mejia (2005), Conducting short duration field programs to evaluate sounding site representativeness and potential climate monitoring biases—Examining the low-level jet over the Venezuelan Llanos during the 2005 dry season, paper presented at 15th Conference on Applied Climatology, Am. Meteorol. Soc., Savannah, Ga.

Durre, I., R. S. Vose, and D. B. Wuertz (2006), Overview of the Integrated Global Radiosonde Archive, *J. Clim.*, *19*(1), 53–68, doi:10.1175/JCLI3594.1.

Ek, M. B., K. E. Mitchell, Y. Lin, E. Rogers, P. Grunmann, V. Koren, G. Gayno, and J. D. Tarpley (2003), Implementations of the upgraded NOAH land-surface model in NCEP operational mesoscale ETA model, *J. Geophys. Res.*, *108*(D22), 8851, doi:10.1029/2002JD003296.

Fiorino, M. (2004), A multi-decadal daily sea surface temperature and sea ice concentration data set for the ERA-40 reanalysis, *ERA-40 Project Rep. Ser. 12*, Eur. Cent. for Medium-Range Weather Forecasts, Reading, U. K.

Grubišić, V., R. B. Smith, and C. Schär (1995), The effect of bottom friction on shallow-water flow past an isolated obstacle, *J. Atmos. Sci.*, *52*(11), 1985–2005, doi:10.1175/1520-0469(1995)052<1985:TEOBFO>2.0.CO;2.

Hamilton, G. D. (1986), National Data Buoy Center programs, *Bull. Am. Meteorol. Soc.*, *67*(4), 411–415, doi:10.1175/1520-0477(1986)067<0411:NDBCP>2.0.CO;2.

Holton, J. R. (2004), The planetary boundary layer, in *An Introduction to Dynamic Meteorology*, chap. 5, pp. 115–138, Elsevier, Burlington, Mass.

Hong, S.-Y., and H.-L. Pan (1996), Nonlocal boundary layer vertical diffusion in a medium-range forecast model, *Mon. Weather Rev.*, *124*(10), 2322–2339, doi:10.1175/1520-0493(1996)124<2322:NBLVDI>2.0.CO;2.

Hong, S.-Y., and H.-L. Pan (1998), Convective trigger function for a mass-flux cumulus parameterization scheme, *Mon. Weather Rev.*, *126*(10), 2599–2620, doi:10.1175/1520-0493(1998)126<2599:CTFFAM>2.0.CO;2.

Huffman, G. J., D. T. Bolvin, E. J. Nelkin, D. B. Wolff, R. F. Adler, G. Gu, Y. Hong, K. P. Bowman, and E. F. Stocker (2007), The TRMM Multisatellite Precipitation Analysis (TMPA): Quasi-global, multiyear, combined-sensor precipitation estimates at fine scales, *J. Hydrometeorol.*, *8*(1), 38–55, doi:10.1175/JHM560.1.

Juang, H. H., and M. Kanamitsu (1994), The NMC nested regional spectral model, *Mon. Weather Rev.*, *122*(1), 3–26, doi:10.1175/1520-0493(1994)122<0003:TNNRSM>2.0.CO;2.

Kain, J. S. (2004), The Kain-Fritsch convective parameterization: An update, *J. Appl. Meteorol.*, *43*(1), 170–181, doi:10.1175/1520-0450(2004)043<0170:TKCPAU>2.0.CO;2.

Kain, J. S., and J. M. Fritsch (1990), A one-dimensional entraining/detraining plume model and its application in convective parameterization, *J. Atmos. Sci.*, *47*(23), 2784–2802, doi:10.1175/1520-0469(1990)047<2784:AODEPM>2.0.CO;2.

Kalnay, E., et al. (1996), The NCEP/NCAR 40-year reanalysis project, *Bull. Am. Meteorol. Soc.*, *77*(3), 437–471, doi:10.1175/1520-0477(1996)077<0437:TNYRP>2.0.CO;2.

Kanamaru, H., and M. Kanamitsu (2007), Scale-selective bias correction in a downscaling of global analysis using a regional model, *Mon. Weather Rev.*, *135*(2), 334–350, doi:10.1175/MWR3294.1.

Kanamitsu, M., W. Ebisuzaki, J. Woollen, S. Yang, J. J. Hnilo, M. Fiorino, and G. L. Potter (2002), NCEP-DOE AMIP-II reanalysis (R-2), *Bull. Am. Meteorol. Soc.*, *83*(11), 1631–1643, doi:10.1175/BAMS-83-11-1631.

Lawrence, M. B., and G. B. Clark (1985), Annual summary—Atlantic hurricane season of 1984, *Mon. Weather Rev.*, *113*(7), 1228–1237, doi:10.1175/1520-0493(1985)113<1228:AHSO>2.0.CO;2.

Magaña, V., J. A. Amador, and S. Medina (1999), The midsummer drought over Mexico and Central America, *J. Clim.*, *12*(6), 1577–1588, doi:10.1175/1520-0442(1999)012<1577:TMDOMA>2.0.CO;2.

Mo, K. C., M. Chelliah, M. L. Carrera, R. W. Higgins, and W. Ebisuzaki (2005), Atmospheric moisture transport over the United States and Mexico as evaluated in the NCEP regional reanalysis, *J. Hydrometeorol.*, *6*(5), 710–728, doi:10.1175/JHM452.1.

Muñoz, E., A. J. Busalacchi, S. Nigam, and A. Ruiz-Barradas (2008), Winter and summer structure of the Caribbean low-level jet, *J. Clim.*, *21*(6), 1260–1276, doi:10.1175/2007JCLI1855.1.

Nigam, S., C. Chung, and E. DeWeaver (2000), ENSO diabatic heating in ECMWF and NCEP-NCAR reanalyses, and NCAR CCM3 simulation, *J. Clim.*, *13*(17), 3152–3171, doi:10.1175/1520-0442(2000)013<3152:EDHIEA>2.0.CO;2.

Rasmusson, E. M. (1967), Atmospheric water vapor transport and the water balance of North America: Part I. Characteristics of the water vapor flux field, *Mon. Weather Rev.*, *95*(7), 403–426, doi:10.1175/1520-0493(1967)095<0403:AWVTAT>2.3.CO;2.

Reed, R. J., D. C. Norquist, and E. E. Recker (1977), The structure and properties of African wave disturbances as observed during phase III

of GATE, *Mon. Weather Rev.*, *105*(3), 317–333, doi:10.1175/1520-0493(1977)105<0317:TSAPOA>2.0.CO;2.

Smith, R. B., A. C. Gleason, P. A. Gluhosky, and V. Grubišić (1997), The wake of St. Vincent, *J. Atmos. Sci.*, *54*(5), 606–623, doi:10.1175/1520-0469(1997)054<0606:TWOSV>2.0.CO;2.

Smith, T. M., R. W. Reynolds, T. C. Peterson, and J. Lawrimore (2008), Improvements to NOAA's historical merged land-ocean surface temperature analysis (1880–2006), *J. Clim.*, *21*(10), 2283–2296, doi:10.1175/2007JCLI2100.1.

Stensrud, D. J. (1996), Importance of low-level jets to climate: A review, *J. Clim.*, *9*(8), 1698–1711, doi:10.1175/1520-0442(1996)009<1698:IOLLJT>2.0.CO;2.

Tiedtke, M. (1989), A comprehensive mass flux scheme for cumulus parameterization models, *Mon. Weather Rev.*, *117*(8), 1779–1800, doi:10.1175/1520-0493(1989)117<1779:ACMFSF>2.0.CO;2.

Tiedtke, M. (1993), Representation of clouds in large-scale models, *Mon. Weather Rev.*, *121*(11), 3040–3061, doi:10.1175/1520-0493(1993)121<3040:ROCILS>2.0.CO;2.

Uppala, S. M., et al. (2005), The ERA-40 re-analysis, *Q. J. R. Meteorol. Soc.*, *131*(612), 2961–3012, doi:10.1256/qj.04.176.

Wang, C. (2007), Variability of the Caribbean low-level jet and its relations to climate, *Clim. Dyn.*, *29*(4), 411–422, doi:10.1007/s00382-007-0243-z.

Wang, C., and D. B. Enfield (2001), The tropical Western Hemisphere Warm Pool, *Geophys. Res. Lett.*, *28*(8), 1635–1638, doi:10.1029/2000GL011763.

Wang, C., and S.-K. Lee (2007), Atlantic Warm Pool, Caribbean low-level jet, and their potential impact on Atlantic hurricanes, *Geophys. Res. Lett.*, *34*, L02703, doi:10.1029/2006GL028579.

Xie, P., and P. A. Arkin (1997), Global precipitation: A 17-year monthly analysis based on gauge observations, satellite estimates, and numerical model outputs, *Bull. Am. Meteorol. Soc.*, *78*(11), 2539–2558, doi:10.1175/1520-0477(1997)078<2539:GPAYMA>2.0.CO;2.

S. C. Chan and V. Misra, Center for Ocean-Atmospheric Prediction Studies, Florida State University, 2035 East Paul Dirac Dr., Rm. 200, Johnson Bldg., Tallahassee, FL 32308, USA. (schan@fsu.edu)

H. Smith, Water Resources Research Institute, University of the Virgin Islands, St. Thomas, VI 00802-9990, USA.